2022-09-29

Reconstructing sedimentary processes in a Permian channellobe transition zone: an outcrop study in the Karoo Basin, South Africa

Pohl, Florian

10.1017/s0016756822000693
Geological Magazine
Cambridge University Press

Geological Magazine

www.cambridge.org/geo

Reconstructing sedimentary processes in a Permian channel–lobe transition zone: an outcrop study in the Karoo Basin, South Africa

F Pohl[1], JT Eggenhuisen[2], J de Leeuw[2], MJB Cartigny[3], HL Brooks[4] and YT Spychala[5]

[1]School of Biological and Marine Sciences, University of Plymouth, Drake Circus, Plymouth PL 4 8AA, UK; [2]Faculty of Geosciences, Utrecht University, P.O. Box 80021, Utrecht, TA 3508, The Netherlands; [3]Faculty of Geography, Durham University, Lower Mountjoy South Road, Durham DH1 3LE, UK; [4]EMR – Geological Institute, RWTH Aachen University, 52062 Aachen, Germany and [5]Leibniz University Hannover, Institute of Geology, Callinstr. 30, 30167, Hannover, Germany

Original Article

Cite this article: Pohl F, Eggenhuisen JT, de Leeuw J, Cartigny MJB, Brooks HL, and Spychala YT. Reconstructing sedimentary processes in a Permian channel–lobe transition zone: an outcrop study in the Karoo Basin, South Africa. *Geological Magazine* https://doi.org/10.1017/S0016756822000693

Received: 21 January 2021
Revised: 7 June 2022
Accepted: 20 June 2022

Keywords:
turbidity current; deep marine; sediment bypass; sediment facies; scour fields

Author for correspondence:
F. Pohl,
Email: florian.pohl@plymouth.ac.uk

Abstract

Turbidity currents commonly bypass sediment in submarine channels on the continental slope, and deposit sediment lobes farther down-dip on the flat and unconfined abyssal plain. Seafloor and outcrop data have shown that the transition from bypass to deposition usually occurs over complex zones referred to as channel–lobe transition zones (CLTZs). Recognition of these zones in cores and outcrop remains challenging due to a lack of characteristic sedimentary facies and structures. This paper focuses on Unit E of the Permian Fort Brown Formation in the Karoo Basin, South Africa, in the Slagtersfontein outcrop complex, which has previously been interpreted as a CLTZ. This study integrates thin-section micrographs, sedimentary facies, bed-set and stratigraphic architecture, and palaeoflow directions to achieve a multiscale analysis of CLTZ features. A novel process-based facies scheme is developed to evaluate deposits in terms of the depositional or erosional tendencies of the flows that formed them. This scheme allows bypass to be distinguished from depositional zones by the spatial distribution of certain sediment facies. Areas of net sediment bypass were predominantly marked by erosive sediment facies and a larger variability in palaeoflow direction while depositional areas showed a lower variability in palaeoflow directions. Metre-scale structures in the bypass-dominated area reveal seafloor erosion and scour formation. Field relations suggest the presence of a ~500 m long mega-scour in the CLTZ. The characteristic structures documented here are applicable for identifying CLTZs in sparse datasets such as outcrops with limited palaeogeographical context and sediment cores obtained from subsurface systems.

1. Introduction

In the deep oceans much sediment is transported by turbidity currents, which are mixtures of sediment and water that flow downslope, driven by gravity (Kuenen, 1937; Lowe, 1982; Altinakar *et al.* 1996; Meiburg & Kneller, 2010). Turbidity currents flow through and create deep-water sediment routing systems that distribute clastic sediments, nutrients, and organic carbon, but also man-made pollutants like microplastics across the continental slope and ocean floor (Galy *et al.* 2007; Mutti *et al.* 2009; Pohl *et al.* 2020*b*). These sediment routing systems are composed of different subsystems, which facilitate the transport or deposition of sediment (Mutti *et al.* 2009; Breien *et al.* 2010; Talling *et al.* 2015; Hessler & Fildani, 2019). For instance, submarine canyons and channels facilitate sediment transport and bypass of turbidity currents (Fildani *et al.* 2013; Stevenson *et al.* 2015), while farther downstream deep-sea fans represent depositional systems where turbidity currents deposit sediment (Normark, 1970; Prélat *et al.* 2009; Stacey *et al.* 2018). In the transition zone between channels and lobes, turbidity currents transform from a net bypassing to a net depositional behaviour. This transformation is commonly associated with a complex zone of erosional and depositional morphologies, often referred to as the channel–lobe transition zone (CLTZ) (Mutti & Normark, 1987; Wynn *et al.* 2002; Ito *et al.* 2014; Hofstra *et al.* 2015; Brooks *et al.* 2018*a*; Pohl *et al.* 2019). CLTZs may represent a potential trapping mechanism for hydrocarbons which might be stored in the sandy lobe deposits farther downstream (Amy, 2019). Thus, understanding of the flow processes and associated structures in CLTZs could help to better assess potential hydrocarbon reservoirs.

The CLTZ was originally defined as the area separating well-defined channels from well-defined lobes and is usually characterized by erosion and sediment bypass (Mutti & Normark, 1987). Bathymetric studies on modern CLTZs on the ocean floor have revealed that these zones can extend for >tens of kilometres, comprising scour fields with individual scours hundreds of metres long and tens of metres deep (Kenyon & Millington, 1995; Palanques *et al.* 1996; Wynn *et al.* 2002; Macdonald *et al.* 2011; Carvajal *et al.* 2017; Maier *et al.* 2020). These

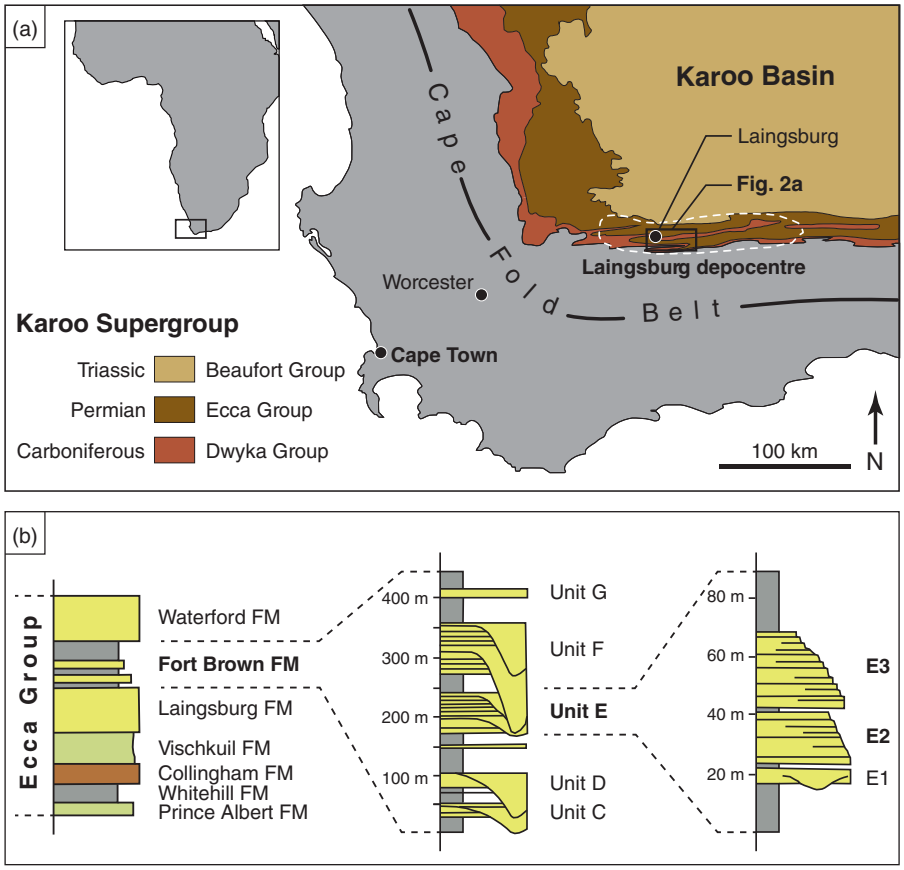

Fig. 1. (Colour online) (a) Location map of the Laingsburg depocentre within the Western Cape (South Africa). Indicated are the main stratigraphic subunits of the Karoo Supergroup. The study area is marked with a black box and shown in Figure 2a. Modified from Flint *et al.* (2011). (b) Lithostratigraphy of the Ecca Group in the Laingsburg depocentre. This study focuses on Units E2 and E3 of the Fort Brown Formation. From HDV Wickens, unpub. PhD thesis, Univ. Port Elizabeth, 1994, and Figueiredo *et al.* (2013). FM: Formation.

types of studies reveal the seabed bathymetry on a metre scale and only allow identification of sediment types and detailed sedimentary structures if they are coupled with sediment coring and/or subsurface seismic-reflection profiles. In contrast, outcrop studies or data from sediment cores can provide detail on small-scale sedimentary structures, but often lack a larger palaeogeographical context. In this paper a detailed multiscale analysis of sedimentary structures and stratigraphic architectures in a documented CLTZ is linked to the net erosive or net depositional behaviour of the turbidity currents that formed these features.

A previously recognized Permian CLTZ in the Karoo Basin, South Africa, reveals erosive patterns in a bypass zone and deposits of an associated lobe complex farther downstream (here referred to as the deposition zone: van der Merwe *et al.* 2014; Brooks *et al.* 2018*a*). The dominant morphological feature controlling the transition from bypass to deposition was interpreted to have been a slope break (Brooks *et al.* 2018*a*), an interpretation that is based on extensive and detailed regional datasets (Hodgson, 2009; Figueiredo *et al.* 2010, 2013; van der Merwe *et al.* 2010, 2014; Flint *et al.* 2011; Hodgson *et al.* 2011; Spychala *et al.* 2015). This body of literature provides an exceptional and independent control on the palaeogeographic interpretation of this exhumed CLTZ, which makes it the ideal study site of sediment types, sedimentary structures and architecture as indicators of turbidity current processes in CLTZs.

Objectives of this study are to: (1) document the characteristic sedimentary structures in the bypass zone on various scales; (2) develop a sediment facies scheme associated with the potential for erosion or deposition; and (3) analyse the palaeoflow distribution in the bypass and the deposition zone.

2. Geological setting

The Karoo Basin in South Africa is a retro-arc foreland basin that was active from the Late Carboniferous to the Early Jurassic (Smith, 1990; Smith *et al.* 1993; Visser & Praekelt, 1996; Visser, 1997; Catuneanu *et al.* 1998; López Gamundí & Rossello, 1998). It is filled with ~5500 m thick sediments of the Karoo Supergroup (Tankard *et al.* 2009; Flint *et al.* 2011), and subdivided into the Dwyka, Ecca and Beaufort Groups (Fig. 1a; e.g. Smith, 1990; HDV Wickens, unpub. PhD thesis, Univ. Port Elizabeth, 1994). This study focuses on the Permian Ecca Group, which comprises a shallowing-upward succession of deep-water to deltaic deposits, recording the eastward progradation of the basin margin (e.g. van der Merwe *et al.* 2010; Flint *et al.* 2011). Provenance analysis of the predominantly fine-grained sandstones of the Ecca Group does not match the signature of the adjacent Cape Fold Belt (Fig. 1a), indicating no nearby source area (Johnson, 1991; Scott *et al.* 2000). Plausible source areas are Palaeozoic granite intrusions in the North Patagonian Massif, as suggested by age constraints and geochemical analyses that indicate a felsic igneous source area associated with an active continental-margin setting (B van Lente, unpub. PhD thesis, Univ. Stellenbosch, 2004; Fildani *et al.* 2007; Flint *et al.* 2011; McKay *et al.* 2018).

The Ecca Group is up to 1300 m thick (van der Merwe *et al.* 2009, 2010 2011) and subdivided into seven formations (Fig. 1b; HDV Wickens, unpub. PhD thesis, Univ. Port Elizabeth, 1994). The upper part comprises the Laingsburg, Fort Brown and Waterford Formations, which are interpreted as sand-prone basin-floor deposits (van der Merwe *et al.* 2010), channelized submarine slope deposits (Di Celma *et al.* 2011; Flint *et al.* 2011; Hodgson *et al.* 2011) and shelf-edge and shelf-top deltas (Jones

https://doi.org/10.1017/S0016756822000693

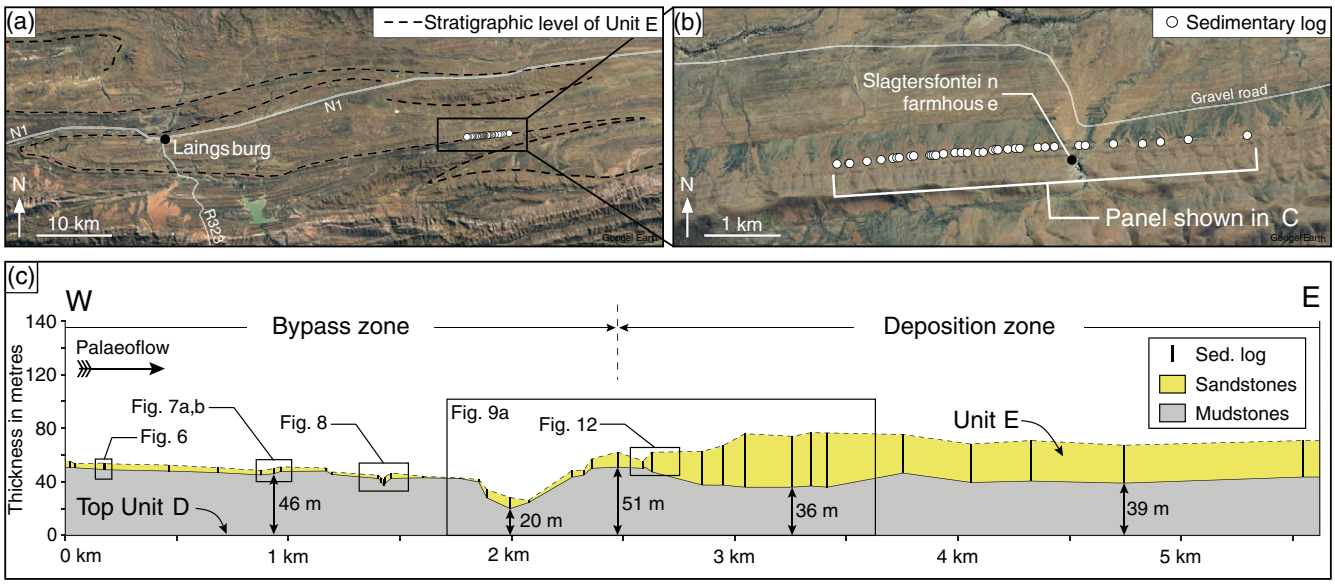

Fig. 2. (Colour online) (a) Satellite photograph showing part of the Laingsburg outcrop area. See Figure 1 for location. (b) Satellite photograph of the Slagtersfontein outcrop area including the locations of the sedimentary logs. Images taken from Google Earth. See Figure 1a for location. (c) Correlation panel of the collected sedimentary logs of Unit E and the thickness to the underlying Unit D. The correlation panel is parallel to the palaeoflow direction. A zone characterized by thin deposits gradually passes, over a downstream distance of ~600 m, into a zone marked by thicker deposits.

et al. 2015; Poyatos-Moré *et al.* 2016). The focus of this study is on the Fort Brown Formation (Fig. 1b).

The deposits of the Fort Brown Formation are characterized, from east to west, by slope valleys, channel–levee systems, intra-slope lobe complexes and basin-floor lobe complexes over a distance of 80–100 km (Figueiredo *et al.* 2010, 2013; Di Celma *et al.* 2011; Spychala *et al.* 2015; Brooks *et al.* 2018*a*, *b*). The slope gradient of the Karoo Basin margin is estimated to have been <0.7° based on reconstructions of the clinoforms in the Waterford Formation (Poyatos-Moré *et al.* 2016). Early research estimated a water depth during deposition of the Fort Brown Formation of <500 m, mainly based on trace fossils (Visser & Loock, 1978). A more recent study, however, estimates the water depth to have been *c.* 1800 m, based on the uncompacted thickness of the succession from basin-floor fans to the first delta deposits (Flint *et al.* 2011). Following the strike dip of the palaeoslope reconstructed by Brooks *et al.* (2018*b*), deepening direction was towards E.

The Fort Brown Formation is subdivided into five units (C, D, E, F and G), each of which is interpreted to represent a low-stand sequence set (Flint *et al.* 2011). The focus of this study is Unit E, which is 40–100 m thick and divided into three cycles (E1, E2 and E3; Fig. 1b). The lowermost unit E1 is only exposed in the northwestern part of the Laingsburg depocentre and interpreted as a set of intra-slope lobes (Spychala *et al.* 2015). Units E2 and E3 comprise tabular, sand-rich bodies, with multiple regional transitions between bypass and deposition and vice versa. The latest interpretation indicates that these transitions between bypass and deposition were controlled by a ramp–step slope geometry, with ~20 km long ramps and steps (van der Merwe *et al.* 2014; Brooks *et al.* 2018*a*, *b*). This interpretation is based on the exceptional control of the regional palaeogeography due to previous studies and the identification of intra-slope lobes (e.g. Figueiredo *et al.* 2010; Spychala *et al.* 2015), showing characteristic features of stepped slope profiles similar to the Niger Delta Slope (Prather *et al.* 2012; Jobe *et al.* 2017) and the northern margin of the Gulf of Mexico (Prather *et al.* 1998, 2012, 2017). The lower bypass zone on the stepped slope, and its downstream transition into a thick composite sandstone body, are exposed in the Slagtersfontein outcrop. Here, the transition from bypass to deposition takes place over a downstream distance of ~600 m, and is characterized by an increase in thickness from a few metres to ~40 m (Brooks *et al.* 2018*a*), an average thickening rate of 0.06 m m^{-1}. This zone is interpreted as a CLTZ with associated lobe deposits related to a slope break (Brooks *et al.* 2018*a*).

3. Methodology and dataset

3.a. The Slagtersfontein outcrop area

Forty sedimentary logs measured on a centimetre scale were collected along a 5.6 km long transect through Unit E in the Slagtersfontein outcrop area (Fig 2a, b). The spacing between individual logs was mainly controlled by the availability of high-quality outcrops in gullies. The position of the base of Unit E was measured with a handheld GPS using a built-in waypoint averaging function that considers errors due to satellite orbit geometry, resulting in a horizontal accuracy of ±2.5 m. The bed-normal distance from the base of Unit E to the underlying Unit D was measured with a 50 m long measuring tape. A correlation panel was constructed, revealing the sedimentary architecture of Unit E in palaeoflow direction (Fig. 2c). The datum level for the correlation panel is the top of the underlying Unit D. This datum was chosen because of minor thickness variations in the study area documented for Unit D (van der Merwe *et al.* 2014; Hodgson *et al.* 2016).

Based on the deposit thickness the outcrop complex is subdivided into two areas. The first comprises the proximal ~2 km of the studied outcrop, is marked by an overall unit thickness of 0 m to ~5 m and is termed the bypass zone (Fig. 2c). The second area is referred to as the deposition zone, with thicknesses of up to ~40 m, and is located downstream of the bypass zone (Fig. 2c).

https://doi.org/10.1017/S0016756822000693

Sedimentary structures up to a scale of several metres were documented with photographic mosaics and detailed sketches. Prior to this, the outcrop was cleaned with a broom to expose detailed structures. A measurement tape was used to ensure geometric accuracy of the sketches.

Only unequivocal and precise flow indicators such as groove and flute marks were measured to reconstruct the palaeoflow directions. The bedding of Unit E in the Slagtersfontein outcrop area is sub-vertical, and the measured palaeoflow directions were corrected for the local bed dip using stereographic projection, and plotted in equal-area rose diagrams (Nemec, 1988; Baas, 2000). Statistical analysis yields the frequency distribution, the mean palaeoflow vector M and the circular standard deviation S_B (Baas, 2000). Palaeoflow results show that the logs are aligned parallel to the palaeoflow direction in the bypass zone and the proximal depositional zone (ENE; ~70°), which allows the investigation of variations in the deposits along the downflow trajectory.

3.b. Sampling and thin-section grain-size analysis

Some of the sediment beds have been selected for detailed grain-size distribution analysis. Sediment beds were selected for sampling based on field relations (e.g. Injectites together with the overlying sandstone) or simply for practical reasons such as suitability for sampling in the field. A total of 44 samples were taken *c.* 3–5 cm above the base of these beds, using either a geological hammer or a drill. The three-dimensional orientation of each sample was documented in the field. From these samples, 30 µm thick thin-sections were prepared, which were oriented perpendicular to the bedding and parallel to the mean palaeoflow direction. Of each thin-section an area of >1 cm^2 (1.27 × 0.95 cm) was photographed using an optical microscope (Leica DM6000 B). Photographs were taken in plane-polarized light with a magnification of 20×. The microscope was equipped with an automated stage to generate a stitched image with a resolution of 13,584 × 10 088 pixels, resulting in a resolution of 1.08 µm per pixel.

The thin-section images were overlain by a grid with a mesh width of 400 µm. The grains that were crossed by a line intersection of the grid were manually outlined using a drawing tablet (Wacom Cintiq 13HD) and the image analysis software ImageJ (Version 1.52a). Preliminary tests revealed that a minimum of 300 grains were needed to obtain a grain-size distribution that was not biased by the number of measured grains. A grain-size distribution obtained from a thin-section is always biased toward a finer grain-size because the centre of an individual grain is rarely located at the intersection of the thin-section surface with that grain. This bias was corrected using the method from Johnson (1994):

$$D' = d' + 0.4(a' - d')^2, \quad (1)$$

where D' is the corrected grain size and d' is equal to $(a'b')^{1/2}$; with a' and b' as the measured long and short axes from the outlined grains. The obtained grain-size distributions were statistically evaluated with standard methods to calculate the sorting (e.g. Boggs, 2009).

4. Results

4.a. Sedimentary facies and structures

The sediments of Unit E in the outcrop complex comprise mainly sandstones, siltstones and mudclast breccias. Sixteen sedimentary facies have been recognized on the basis of lithology, grain size, texture and sedimentary structures (see Figs 3 and 4). These sedimentary facies and structures are interpreted and classified with regard to the erosive/depositional tendency of the parent turbidity currents at the time of their formation. Facies descriptions and interpretations are provided in Table 1.

4.b. Sedimentary facies ranking scheme

Here, we organize the sedimentary facies by the erosive or depositional tendency of the turbidity currents from each of the facies. This approach contrasts with the conventional grouping in facies associations, groups of co-occurring facies in outcrops. The suite of physical, biological and chemical processes that can be interpreted from the facies association can then lead to an interpretation of the depositional environment in which it was formed. An example for the application of this type of facies scheme to the present outcrops can be found in Brooks *et al.* (2018*a*). Here, the facies are ranked according to the erosional or depositional tendency of the parent turbidity currents (Fig. 5). Sedimentary facies that were not related to flow processes and predominantly related to background sedimentation or distal turbidity currents are not included in this facies ranking. The remaining 13 facies were sorted into six groups and colour-coded according to the erosion strength or depositional tendency of the flows that created them (Fig. 5). This colour scheme is used in later panels to illustrate the facies distribution, and hence the turbidity-current behaviour.

4.c. Bed-scale structures in the bypass zone

Bed-scale structures in the bypass zone are characterized by deformed sediment beds, rip-up of the seabed and chaotic deposition. Figure 6 shows a deformed sandstone bed (F6) with folded mudstones (F1 and F2) underneath. In other locations erosive surfaces cut down into the underlying sediments, forming troughs and irregularities on the ocean floor, filled with a chaotic mixture of ripped sandstone beds (F6, F11 and F14) and mudclast breccias (F16) (Fig. 7a, b).

4.c.1. Interpretation

The bed-scale structures in the bypass zone are dominantly related to erosion and sediment bypass, suggesting mainly erosive turbidity currents in that zone. These flows are intercalated with the fine hemipelagic deposits deforming and eroding previous deposits and cause rip-ups of the seabed (Figs 6 and 7). The rip-up structures represent bed defects which may have led to the establishment of large-scale scours. The overturned sandstone bed was likely eroded further upstream, dragged and overturned by the flow and deposited at this location (Fig. 6). Comparable deformation structures (i.e. folded beds) have been described in sediment beds underneath mass-transport complexes (Ogata *et al.* 2012). Alternatively, the sandstone beds might have been deformed by slide events caused by restricted collapses that were probably related to local oversteepening of the bed slope.

4.d. Large-scale sedimentary structures and architecture

4.d.1. Incision in the bypass zone

In the bypass zone the sediment of Unit E fills a ~2 m deep incision into the underlying mudstone (F1) over a downstream distance of ~25 m (Fig. 8). The incision is filled with massive mostly structureless sand (F6, F9, F10) with floating mudclasts (F14). The contact of this sandstone with the underlying mudstone is sharp and undular and

https://doi.org/10.1017/S0016756822000693

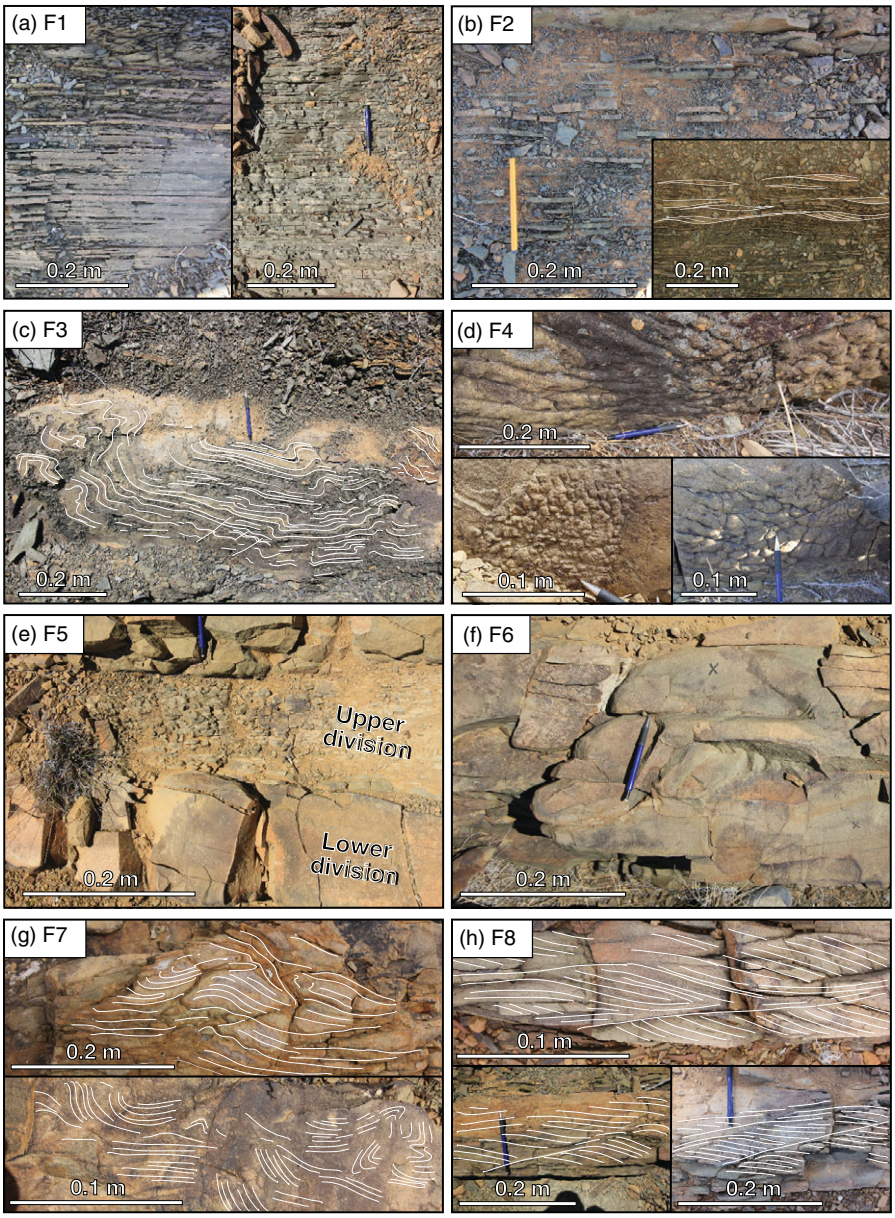

Fig. 3. (Colour online) (a) Thin-bedded mudstones. (b) Tabular thin-beds. (c) Slumped units. (d) Sandstones with loaded bed-bases. (e) Hybrid beds. (f) Structureless sandstone. (g) Convoluted beds. (h) Climbing-ripple cross-laminated sandstone.

interpreted as an erosive surface. The sandstone is draped by a ~10 cm thick mudclast breccia (F16; Fig. 8). The mudstone below the incision is affected by injected sand (F15; Fig. 8). Injectites are also present up- and downstream of the scour. The massive sandstone filling the incision is overlain by a sandstone (F7 and F8) with large-scale backsets that are up to ~1.5 m thick (Fig. 8). Downstream of these backsets, beds are wavy with a wavelength of ~3 m to 5 m and a wave-amplitude of ~1 m. Both the backsets and the wavy beds are truncated by a continuous major erosion surface producing an undular contact that is overlain by a mudclast breccia (F16).

Differences in grain-size distribution between the injectites and the overlying sandstone do unravel their correlation. The grain size of the injected sand is *c.* 40 µm coarser than the overlying sandstone at the same location, suggesting no link of the injected sand to the sand that was deposited on top of it (Fig. 8). The injected sand underneath and downstream of the incision is slightly coarser-grained than the injectite upstream of the incision. The sandstone filling the incision has a similar grain size to the sandstone forming the backsets and the wavy beds, with the difference that the grain-size distribution of the incision infill is slightly coarse-tailed. The sandstone upstream of the incision shows a slight shift toward a finer grain-size distribution (see blue grain-size distribution curve in Fig. 8).

4.d.2. Thinning of the mudstone package underneath Unit E

The hemipelagic mudstones (F1) that separate the sandstones of Unit E from the underlying sandstones of Unit D shows an average thickness ranging from ~35 m to ~50 m (Figs 2c, 9a). However, the thickness of the mudstone package is reduced to a minimum of ~20 m at the end of the bypass zone. Thickness decreases over a downstream distance of ~150 m to its minimum and increases to its normal thickness of ~43 m over a downstream distance of ~350 m, resulting in an asymmetric trough shape with a length of ~500 m and a depth of ~25 m (Fig. 9a). This asymmetric trough shape was also captured by the GPS points and is noticeable as an offset of the base of Unit E from its general stratigraphic level (Fig. 10). By contrast, the satellite images show a continuous, straight stratigraphic level for the sandstones of

https://doi.org/10.1017/S0016756822000693

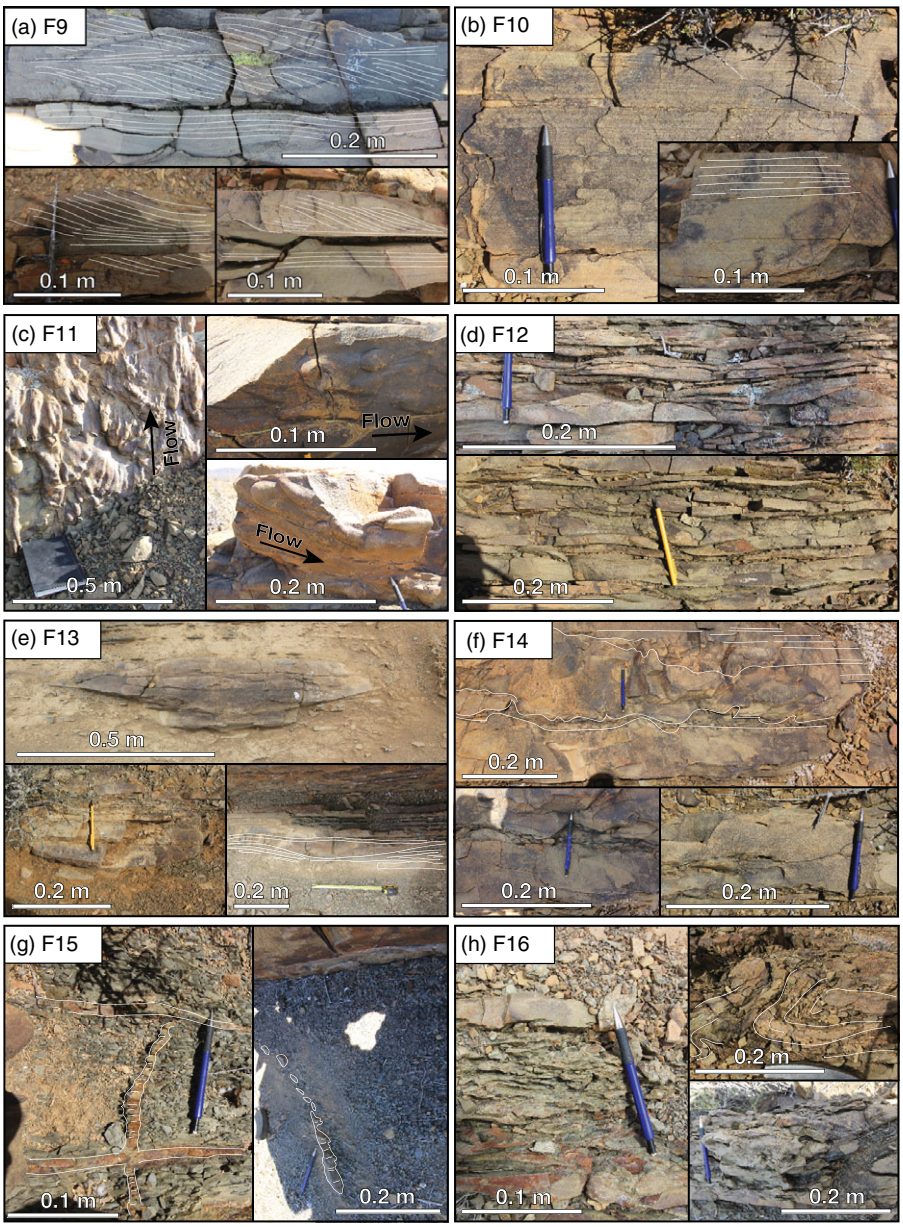

Fig. 4. (Colour online) (a) Ripple-laminated sandstone. (b) Laminated sandstone. (c) Sandstone with flute marks. (d) Lensoid packages. (e) Filled dish-shaped scours. (f) Amalgamated beds with mud-clast horizons. (g) Injectites. (h) Mudclast breccia.

the underlying Unit D along the entire length of the outcrop (Fig. 10).

Upstream of the zone with the thin mudstone area, i.e. in the bypass zone, Unit E is less than 1 m thick and characterized by sedimentary facies indicating scouring and erosion such as mudclast breccia (F16) and injectites (F15) (Injectite in Fig. 9a). On top of the thin mudstone area, the deposits of Unit E are up to ~8 m thick (zone with thin mudstones in Fig. 9a). At the base is an up to 4 m thick package of thin-bedded and fine-grained sandstones (F2) that are overlain by a structureless up to 3.5 m thick sandstone (F6). Farther downstream, the thickness of the deposits of Unit E increases to ~12 m and the sediments are dominated by depositional sedimentary facies (i.e. F4–F10) (Deposition zone I in Fig. 9a).

Variations in deposit thickness and the sediment facies between the different zones are also reflected in the average grain-size distribution of the sediment beds (Fig. 9). Samples for grain-size analysis have been taken from injectites upstream, and from sediments at two locations downstream of the zone with thin mudstones (Figs 9a, b, 11). Grain-size measurements of the injectites upstream revealed a very fine to fine grain size with moderately good sorting (Figs 9b, 11). The sandy deposits on top of the thin mudstone are slightly finer than the upstream injectites and poorly sorted. The sediments deposited ~0.6 km farther downstream of the zone with thin mudstones, i.e. in the deposition zone, were finer-grained with a poor sorting (Figs 9b, 11). The grain-size distribution ~1.4 km downstream of the thin mudstone zone revealed a similar grain size in combination with a moderate sorting.

4.d.3. Transition from the bypass to deposition zone

The transition from bypass to deposition zone is marked by a thickness increase of the Unit E sediments from ~5 m to ~ 40 m over a downstream distance of ~600 m (Fig. 2). The contact of the Unit E sediments with the underlying mudstones (F1) is generally non-erosive, with exceptions at some locations, where the base of Unit E is undular and the underlying mudstones are

https://doi.org/10.1017/S0016756822000693

Table 1. Description and interpretations of the 16 sediment facies.

Facies		Facies description	Facies interpretation
F1	*Thin-bedded Mudstones*	Grey to greenish, thin-bedded mudstones. Beds are <1 cm to m´s thick with sharp, flat to (rarely) wavy boundaries (Fig. 3a). The mudstones are occasionally interbedded with siltstone beds that are <0.5 cm thick. Individual beds are traceable laterally over several meters.	Background hemipelagic deposits deposited in the absence of sand supply. The siltstone beds are deposits of distal dilute turbidity currents.
F2	*Tabular thin-beds*	Packages of grey mudstones intercalated with yellowish to ochre thin-beds of siltstone and very-fine sandstone (Fig. 3b). Packages are between ~10 cm to several meters thick. Individual siltstone and sandstone beds are between <0.5 cm to ~3 cm thick and have a sharp boundary with the over- and underlying mudstone. Bed bases are flat and tops are commonly wavy. Some of the wavy beds show cross lamination and/or starved ripple lamination (Fig. 3b). Individual beds are traceable laterally over 10s of centimetres up to several meters.	The mudstone beds likely represent hemipelagic background deposits or the Te-division of Bouma sequences (Bouma, 1962). The siltstone and sandstone beds are interpreted to have been deposited from dilute turbidity currents. Sharp bed bases, without any irregularities, indicate deposition by non-erosive flows. Wavy tops and ripple lamination indicate deposition from weak flows in the lower flow regime (Baas, 1994; Mulder & Alexander, 2001). The presence of starved ripples suggests a net decrease in current speed and deposition, resulting in the depletion of the flow in suspended sediment load (Reineck & Singh, 1980; Collinson, Mountney & Thompson, 2006).
F3	Slumped units	Localized tightly folded and contorted packages of mudstones (F1) or tabular thin-beds (F2). The thickness of the slumped units ranges from ~0.3 m to >3 m and individual beds within these units are still intact (Fig. 3c). Minor faults are locally present with an offset of ~0.5 cm to ~5 cm. The slumped units can be traced laterally over ~1 m to ~10 m after which they grade into undeformed beds.	The slumped units are interpreted to represent local remobilization of previously deposited sediment as slumps and slides.
F4	*Sandstones with loaded bed-bases*	Fine-grained, ochre-coloured sandstone beds with a thickness of ~0.3 m to ~1.9 m and bed bases that imprint ~1 cm to ~10 cm deep into the underlying mudstones (Fig. 3d). Loading structures cover the full bed-base surfaces and have a rounded and bulbous shape. The thickness of individual beds is between 3 cm to 1 m and the grainsize is fine to medium.	The loading structures are interpreted to have been formed by a suddenly imposed load on the underlying mudstones. Rapidly deposited sand has a higher density than mud due to differences in porosity (30-50% in sand vs. 40-70% in mud (Earle, 2019)) . As a consequence the sand tends to sink into the underlying mud forming loading structures (Collinson, Mountney & Thompson, 2006). Thus, the loading structures indicate rapid deposition from depletive or collapsing flows.
F5	Hybrid beds	Bipartite beds consisting of an ochre-coloured lower sandstone division and a greyish, finer grained upper division (Fig. 3e). The lower division is composed of very-fine to fine-grained sandstone with a sharp base and a thickness of ~10 cm to ~40 cm. The sandstone is generally structureless but shows occasional mudclast horizons or floating mudclasts in the upper third of the bed. The boundary to the overlying upper division is sharp, commonly undular and wavy. The upper division is a siltstone with a thickness of ~5 cm to ~30 cm that is commonly thinner than the associated underlying lower division. The lower part of the siltstone often contains floating mudclasts and isolated sand grains floating in the silt-sized matrix. The mudstone contend of the units varies between 10 to 60%.	The bipartite beds are interpreted as a type of hybrid event bed (Haughton, Barker & McCaffrey, 2003; Haughton *et al.* 2009). The lower division was deposited from a sand-rich high-density turbidity current and the upper division from a genetically linked cohesive debris flow. Hybrid event beds formed by the up-dip entrainment of mud and mudclasts into a sand-bearing turbulent flow, resulting in the damping of turbulence and the development of high-concentration to pseudo-laminar flow conditions (Haughton, Barker & McCaffrey, 2003; Talling *et al.* 2004; Haughton *et al.* 2009). This effect caused rapid sediment deposition from the flow once it became depositional.
F6	*Structureless sandstone*	Individual beds of structureless sandstone are generally >20 cm thick (rarely up to >2 m). The grain size is very fine to medium sand with rare normal grading in the upper part of the beds. Individual bed bases and tops are sharp and flat. The sandstone lacks any visible internal structures (Fig. 3f).	These beds were possibly deposited from sand-rich high-density turbidity currents (Lowe, 1982; Kneller & Branney, 1995). The lack of internal structures together with the thickness of the beds indicates rapid deposition.
F7	*Convolute beds*	Very-fine to fine sandstone beds with a thickness of ~0.3 m to ~1.6 m and an average thickness of ~0.5 m (Fig. 3g). The beds have sharp and flat bases and undular and contorted tops. The main feature of this facies is the folding and deformation of the internal lamination and the bedding structure.	The contorted structure of this facies was produced by soft-sediment deformation during and immediately after deposition of the beds. Soft-sediment deformation can be caused by loss of strength during dewatering of the sandy bed (Mulder & Alexander, 2001; Talling *et al.* 2012). Rapid deposition from depletive or collapsing flows would result in a large pore space and, therefore, excess water in the deposited sand. Convolute lamination and bedding is therefore interpreted to indicate high rates of deposition (Allen, 1972; Kneller, 1995).

(*Continued*)

Table 1. (*Continued*)

Facies		Facies description	Facies interpretation
F8	*Climbing-ripple cross-laminated sandstone*	Fine-grained sandstone beds with climbing-ripple cross-lamination (Fig. 3h). Bed thickness is between ~5 cm to ~21 cm with sharp and flat bases and tops. Climbing ripple lamination locally exhibits a high angle of climb, ~15° to ~30°, and stoss-side preservation of laminae. The lower part of the sandstone beds is structureless.	Climbing ripples occur when suspended sediment load fallout and bedload transport occur simultaneously. The angle of ripple climb reflects the sediment aggradation rate (Allen, 1970; Allen, 1973; Jobe, Lowe & Morris, 2012). We interpret this facies to reflect high sediment fallout rates from depletive or collapsing turbidity currents.
F9	*Ripple-laminated sandstone*	Very fine to fine-grained, ochre sandstone beds with cross stratification. Thickness of individual beds is generally <10 cm, but may reach up to ~25 cm. The cross lamination is predominantly situated toward the top of the beds while the lower part often shows parallel lamination (Fig. 4a). Bed bases are generally sharp and bed tops are sharp and commonly wavy. Rarely normal grading is visible in some of the beds. The lower part of the sandstone beds is structureless.	Cross lamination together with parallel lamination (Bouma Tb and Tc) suggest deposition by turbidity currents at moderate sediment fallout rates (Bouma, 1962; Lowe, 1982; Mutti *et al.*, 1999).
F10	*Planar- Laminated sandstone*	The very fine to fine grained and ochre sandstone beds of this facies have a thickness of ~10 cm to ~20 cm. Some of the beds are up to 75 cm thick. The beds have sharp and flat tops and bases. Bed bases are wavy in some places. Planar-parallel lamination occurs predominantly in the upper third of the beds (Fig. 4b). The lower part of the sandstone beds is structureless.	The beds are interpreted to have been deposited by turbidity currents as Td Bouma intervals, indicating a low-energy flow regime (Bouma, 1962; Mutti, 1992; Mutti *et al.*, 1999).
F11	*Sandstone with flute marks*	Fine-grained sandstone beds, ~5 cm to ~65 cm thick, with flute marks at the base. The flute marks are arranged in clusters and the length of individual flutes ranges from ~3 cm to ~30 cm (Fig. 4c). Most of the flutes show a parabolic-narrow or spindle shape (Allen, 1971). The grainsize between individual beds varies between fine to medium-grained sand and the bed thickness is between 2 cm to 50 cm.	The flute marks are interpreted to have been formed by bypassing flows. These flows have been strong enough to erode into the underlying mudstone, forming scour marks (Allen, 1971). The scours may have been filled by the same flow event, but at a later stage when the flow was waning and depositional. The scours may also have been filled with sediment deposited by subsequent flows.
F12	*Lensoid packages*	10s of cm thick packages containing ~0.5 cm to ~3 cm thick very fine to fine-grained sandstone beds intercalated with thin <0.5 m mudstones (Fig. 4d). The sandy beds have a wavy and lenticular shape with some of the beds pinching out laterally over a distance of 10s cm (in the paleoflow direction). Individual sandstone beds have sharp bases and tops and generally no recognizable internal structures; however, some beds show cross-lamination. The thin mud layer, separating the individual sandstone beds also varies in thickness laterally.	We interpret the lensoid packages to represent alternating phases of bypass and deposition. These beds were likely deposited by turbidity currents that were close to the threshold of either depositing or to bypassing sediment, resulting in the alternating structure of thin beds within the sandstone packages and the lenticular shape of individual beds.
F13	*Dish-shaped scour-fill*	Lensoid, fine-grained sandstone beds that cut into the underlying mud (Fig. 4e). Individual dish-shaped structures are several 10s cm in length and cut ~5 cm to 20 cm deep into the underlying mud. The dish-shaped structures are symmetrical and pinch out laterally. The only visible internal structure is a weakly developed lamination which follows the downcutting shape of the dish-shaped structure.	The dish-shaped incision was probably formed by erosion underneath a dominantly bypassing turbidity current. The fill of the dish structures is interpreted to represent lag deposits of a bypassing turbidity current, where the sediment was trapped in the depression.
F14	*Amalgamated beds with mudclast horizons*	Fine-grained sandstone beds with an irregular and erosive base and top and a thickness of ~5 cm to ~60 cm (Fig. 4f). Individual beds have several sub-horizontal amalgamation surfaces, indicated by a thin <1 mm layer of mud or silt. Some of the amalgamation surfaces are cutting down through underlying amalgamation surfaces. A very common feature in this facies are undular mudclast horizons with abrupt lateral thickness variations between ~1 cm to ~10 cm (Fig. 4f). Mudclasts within these horizons are <1 cm to ~7 cm in size.	The amalgamated sandstones are interpreted as deposited by several successive flow events, likely high-density turbidity currents (Lowe, 1982; Kneller & Branney, 1995; Mulder & Alexander, 2001). Flows have partly reworked and eroded the underlying sediment that had been deposited by previous flows (e.g. mudclast horizons), indicating erosive and bypassing flows (Lien, Midtbø & Martinsen, 2006).

(*Continued*)

Table 1. (*Continued*)

F15	*Injectites*	Injectites are composed of fine- to medium-grained sand and were injected into the underlying mudstones (Fig. 4g). The injectites are ~1 cm to ~5 cm in width and individual injectites range up to ~1.5 m deep into the mudstones. The injectites are oriented either sub-vertical or horizontal relative to the local bed orientation, forming dykes and sills respectively.	The injectites are interpreted to have been injected into the underlying mudstone by an overriding turbidity current. Injectites by sediment gravity flows into the underlying substrate have been documented by other studies (Parize & Fries, 2003; Butler & McCaffrey, 2010; Eggenhuisen *et al.*, 2011; Ogata *et al.*, 2014). An alternative mechanism for the formation of injectites is post-depositional emplacement due to pore fluid overpressure in buried unconsolidated sedimentary bodies sealed within less permeable sediments (Hurst *et al.*, 2003; Kane, 2010; Cobain, Peakall & Hodgson, 2015; Cobain *et al.*, 2017). However, comparison of the grain-size distribution of the injectites with the sediment on top of it revealed clear differences, implying that the overlying sandstones are not the parent body of the injectites.
F16	*Mudclast breccia*	Chaotically mixed and internally deformed deposits of sand and mudclast breccias (Fig. 4h). The thickness of these deposits ranges from ~5 cm to >1 m. The bases are erosive and both the bases and tops are undular. Individual mudclasts have a size of ~1 cm to 10 cm and are often horizontally aligned. In some locations packages of intact beds are folded and ductilely deformed.	The mudclast breccia is interpreted as the result of multiple flow events. The mixture of rip-up mudclast and sandstone beds indicates that sediment was eroded and reworked by highly erosive flows, likely high-density turbidity currents. Similar facies have been described at the erosive margins of submarine channels (e.g. Hubbard *et al.*, 2014).

deformed (Fig. 12). The bed architecture shows that the beds in the lower part of Unit E are cut off by an erosive surface that is dipping upstream (Fig. 12). The erosive surface is draped by a mudclast breccia (F16), which is overlain by sandstone beds (F6) with an upward-thinning pattern. The sandstones overlying the mudclast breccia are thinning in the upstream direction. The sandstones at the top of Unit E are overlain by hemipelagic mudstones (F1).

4.e. Palaeoflow distribution

One hundred and eighty-four palaeoflow indicators were measured in the outcrop complex. For this study, only unequivocal and precise palaeoflow indicators (i.e. groove and flute marks; Fig. 4c) were used. Groove marks were found at the base of sediment beds from various sediment facies while flute marks were, by definition, only present in facies F11 – sandstone with flute marks. Palaeoflow measurements were divided into three populations based on their downstream location: the bypass zone, the proximal and the distal deposition zone (Figs 13, 14). The mean palaeoflow direction in the bypass zone and in the proximal deposition zone is toward the ENE (~70°), and hence, the W–E correlation panel is oriented broadly parallel to the palaeoflow direction. Farther downstream, however, in the distal deposition zone, the mean palaeoflow direction has changed toward the NNE (Fig. 13). The circular standard deviation s_B describes the variability of the measured vectors and thus the palaeoflow direction. The data show a higher variability in palaeoflow direction in the bypass zone than in the deposition zone (Fig. 13).

5. Discussion

The aim of this study is to identify sedimentary facies, sedimentary structures and stratigraphic architectures, which can help to identify CLTZs in datasets with limited palaeogeographical context. The CLTZ exposed in the Slagtersfontein outcrop area reveals a complex pattern of both erosive and depositional structures on various scales. This diversity of sedimentary structures makes it difficult to pinpoint a single feature to characterize zones of predominant erosion and sediment bypass. Here, we demonstrate how a process-based sediment facies scheme can be used to distinguish zones of bypass from zones of deposition solely by the distribution and frequency of sediment facies. In addition, a process-based reconstruction of the sedimentary structures and stratigraphic architectures shows how net erosional processes can result in complex patterns of erosional and depositional structures. Finally, the variability of the palaeoflow direction may also serve as a possible criterion to distinguish zones of bypass from zones of deposition.

5.a. Distribution of the sedimentary facies

The definition of sedimentary facies is a method which is commonly used to describe and interpret sedimentological datasets ranging from basin scale down to individual sediment cores (e.g. Anderton, 1985; Pickering *et al.* 1986; Reading, 1996). Usually, individual sedimentary facies are defined on sedimentary features such as grain size, fabric and bed-internal structures, and associations of these sedimentary facies are then linked to a particular depositional environment (e.g. Brooks *et al.* 2018*a*). Thus, environments dominated by deposition are linked to different

https://doi.org/10.1017/S0016756822000693

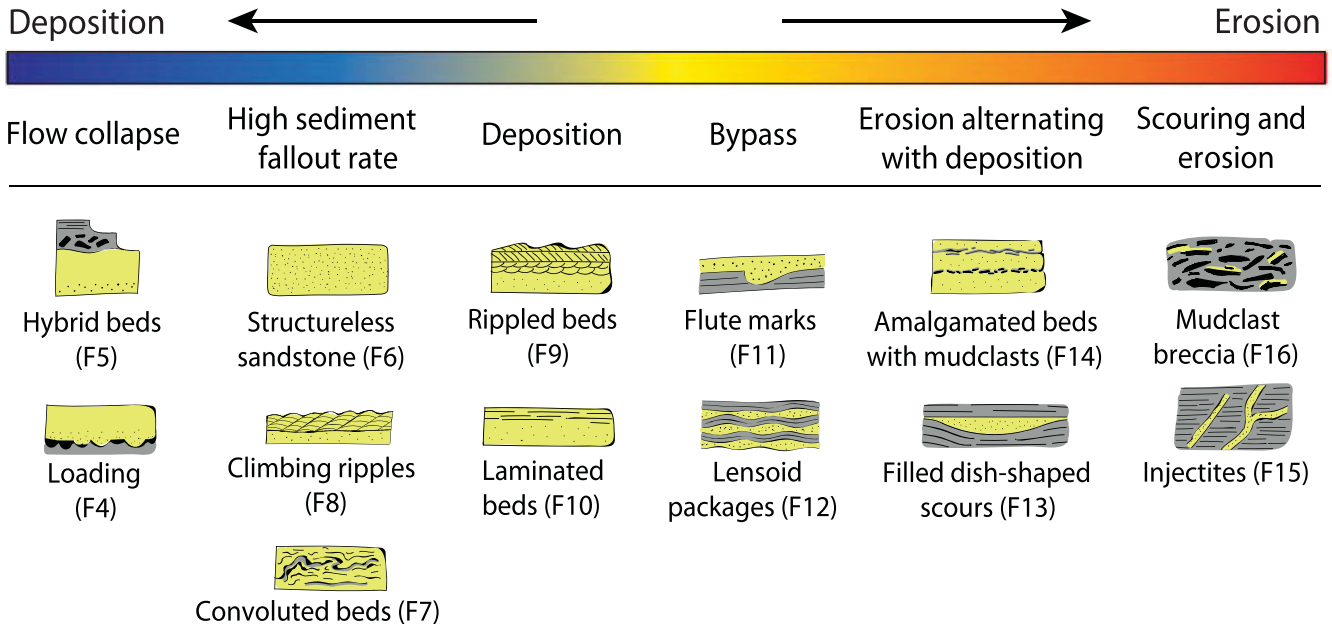

Fig. 5. (Colour online) Facies ranking according to the erosion strength or depositional tendency of the flows.

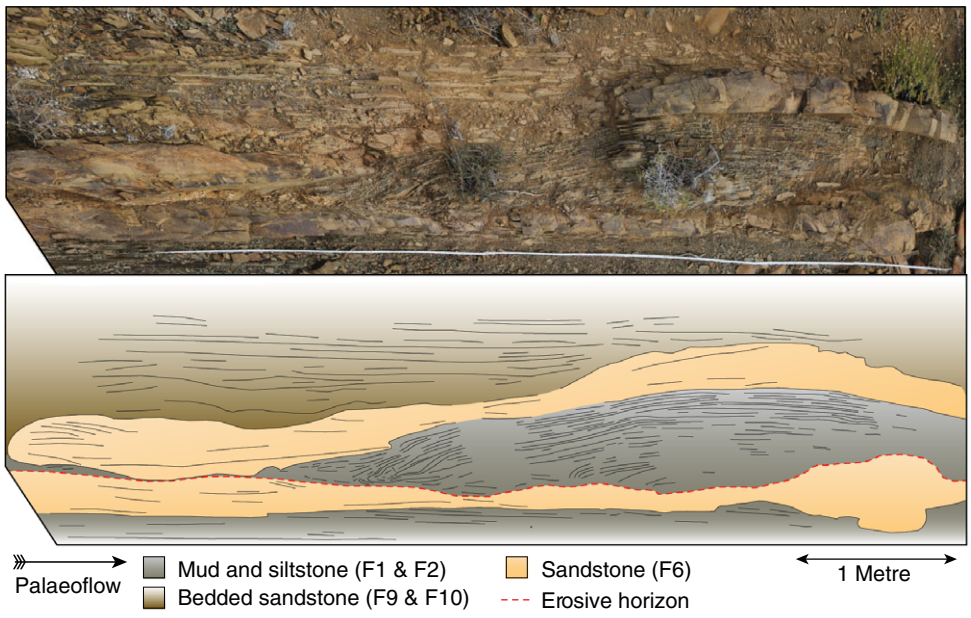

Fig. 6. (Colour online) Deformed interval within the deposits of the bypass zone. The lower one of the two sandstones shows an irregular and erosive top. On top of that erosion surface lies a deformed muddy interval with a discontinuous sandstone on top. See Figure 2 for location.

facies associations than environments dominated by bypass and erosion. However, this relation may become obscure in environments marked by both erosive and depositional structures, which is common in areas marked by scours and seafloor erosion. As such, alternations of erosive and depositional facies have been recognized in sediment cores from the Navy Fan and the La Jolla Fan systems (Carvajal *et al.* 2017; Maier *et al.* 2020; Fildani *et al.* 2021), as well as in studies on CLTZs in outcrops (Gardner *et al.* 2003; Pemberton *et al.* 2016; Navarro & Arnott, 2020). In settings characterized by complex patterns of erosion and deposition, a distinct link of facies associations to this environment might be difficult and interpretation would benefit from a process-oriented facies classification approach like the one presented here (5).

For this study a sediment facies scheme was employed based on the erosional strength or depositional tendency of the flows. This facies scheme allows identification of zones of bypass or deposition not only based on the architecture of the outcrop complex (i.e. unit thickness; Fig. 2), but on the spatial distribution and frequency of certain sediment facies. The advantage of this approach is that it may allow zones of bypass or deposition in datasets with limited information to be identified. Figure 14 illustrates the spatial distribution of the sediment facies and, in consequence, the spatial distribution of erosive and depositional flows in the outcrop complex. The facies distribution in the bypass zone is marked by alternating erosive and depositional sedimentary facies. A high degree of spatial variability over short length scales turns out to be a defining

https://doi.org/10.1017/S0016756822000693

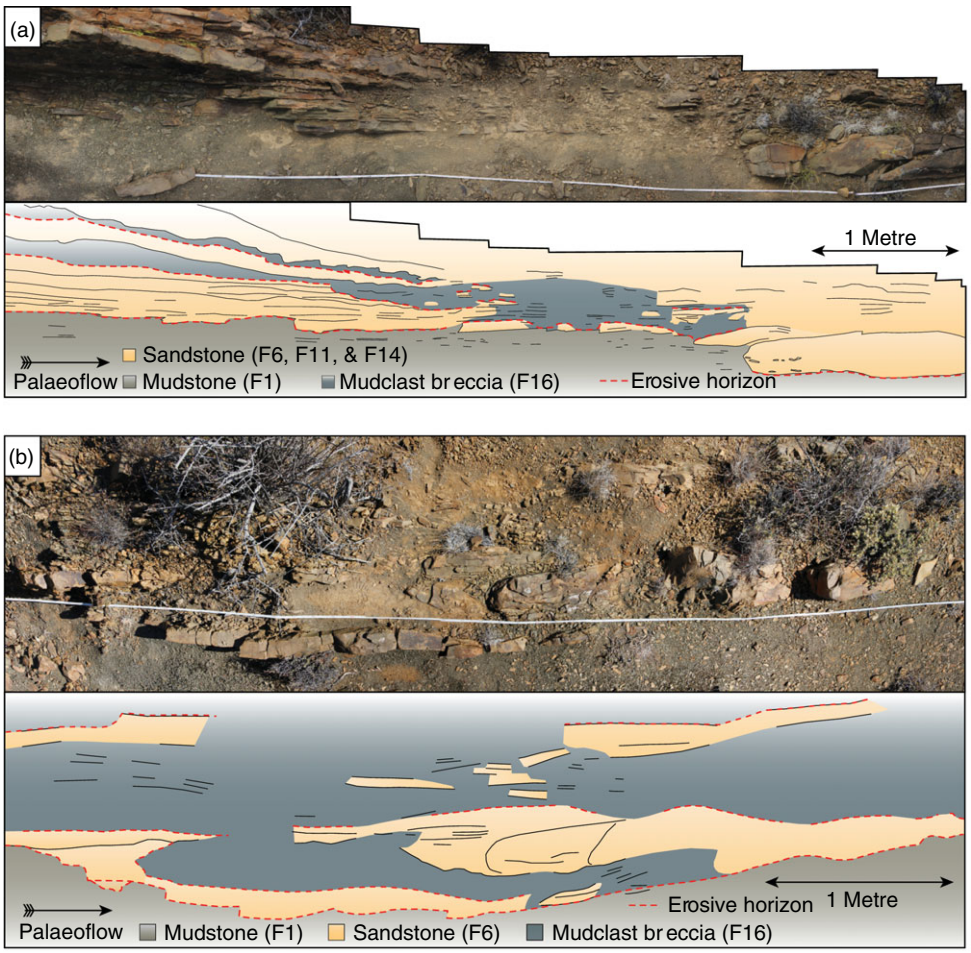

Fig. 7. (Colour online) (a) Surfaces that are cutting down into the underlying sand deposit of previous flows. (b) An erosive surface forming a trough filled with a chaotic mixture of sandstone beds and mudclast breccia. See Figure 2 for location.

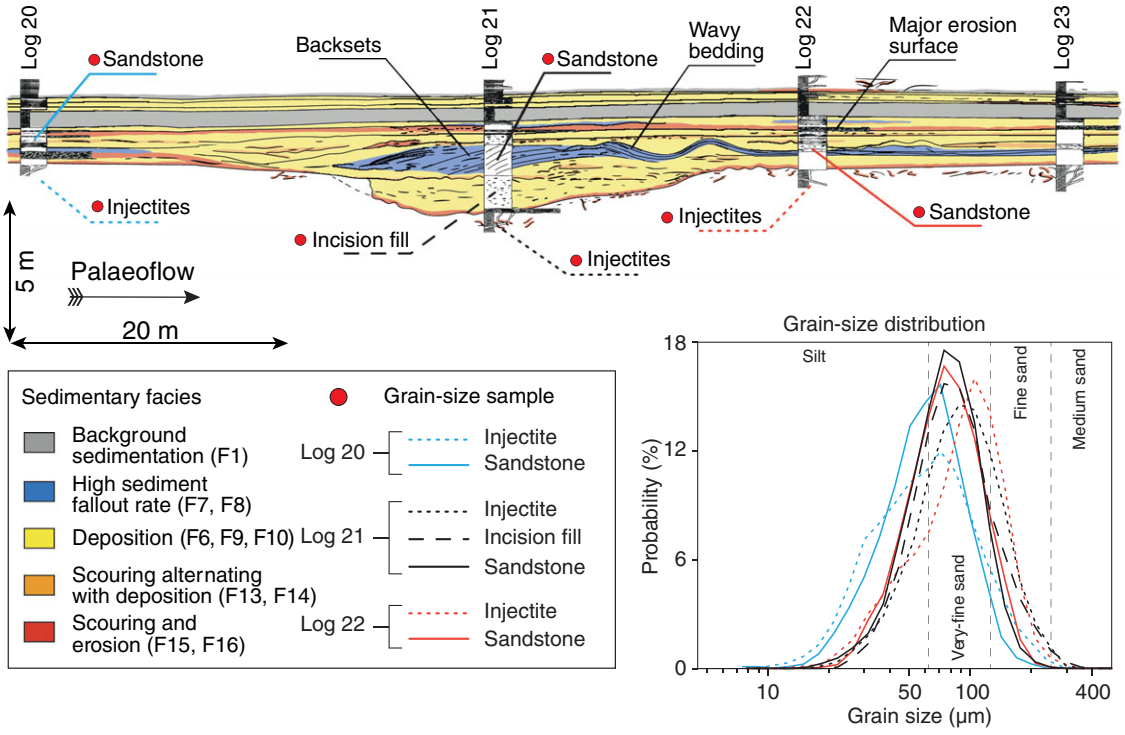

Fig. 8. (Colour online) Incision in the bypass zone (see Fig. 2 for location). The incision is ~2 m deep and ~25 m long and cuts into the underlying hemipelagic mud. The erosive horizon at the base of Unit E is marked by injectites. The incision is filled with structureless sandstone with floating mudclasts. Large-scale backsets and wavy beds are on top of the sandstone filling the incision. Sample positions for grain-size analysis are indicated with red dots.

https://doi.org/10.1017/S0016756822000693

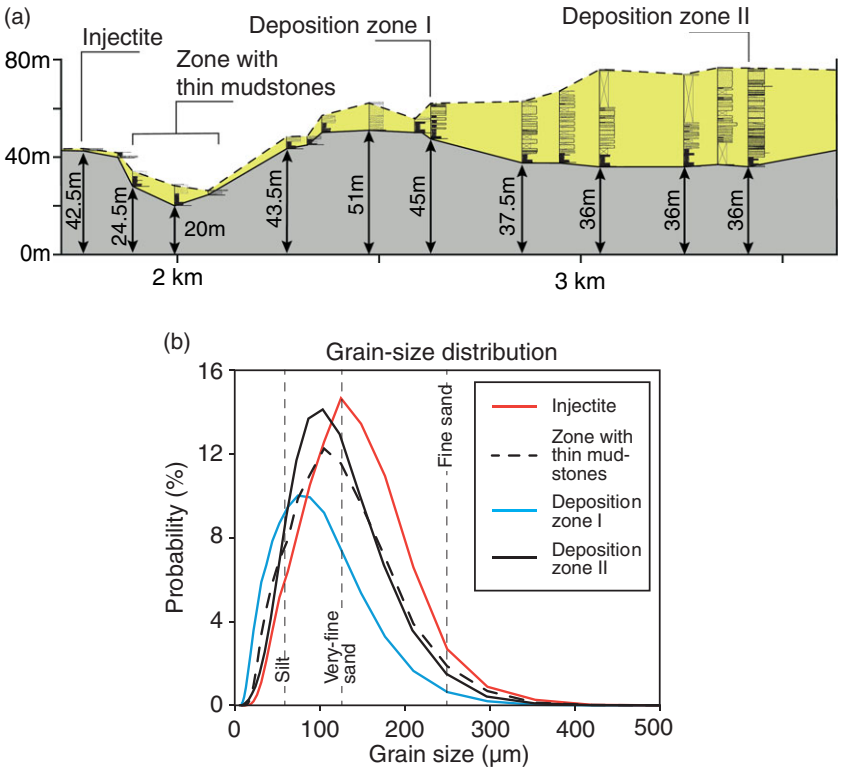

Fig. 9. (Colour online) (a) Correlation panel of the zone with thin mudstones, with sampling locations indicated (see Fig. 2 for location). (b) Grain-size distribution of the sediment at the location indicated in the correlation panel. The average grain-size distribution of all samples taken in that location is displayed. The grain-size distribution of the individual samples is shown in Figure 11.

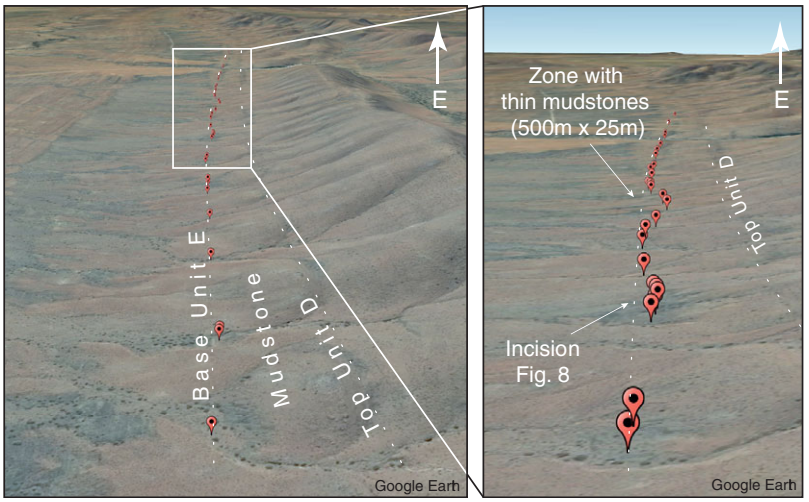

Fig. 10. (Colour online) GPS-points captured at the base of Unit E of each measured section. View toward the east. Noticeable in the GPS data is an offset from the general stratigraphic level of Unit E, while the stratigraphic level of Unit D remains constant.

characteristic of the studied CLTZ. This variability may even express strongly differencing erosive and depositional tendencies within single flow events, though the complexity prevents identification of event beds over the necessary distances to confirm this. The transition from bypass to deposition zone is characterized by a rapid thickness increase of Unit E from ~5 m to ~40 m over a distance of ~600 m. This increase in thickness is accompanied by the transition from erosive to predominantly depositional facies (Fig. 14).

Various approaches to facies classification of turbidite deposits have been applied in literature previously. Many studies of specific stratigraphic successions have tailored classifications at specific deposits and research questions. Some have proven useful more generally, and these have gained broader use in literature. We will compare our facies approach to two notable schemes in use (Lowe, 1982; Mutti, 1992).

Mutti (1992) devised a facies scheme containing nine facies. This classification scheme is organized along the interpreted flow-rheology and sedimentary process of the parent flows. F1–F9 cover deposit types formed by the entire breadth of gravity flow processes from cohesive debris flows to low-density subcritical turbidity currents. Rapid deposition as well as erosion is present in facies F2–5, F7 and F8. Only cohesive debris flows (F1), cross-strata near the top of beds (F6) and (cross-)laminated sandstones (F9) are devoid of indicators of erosion or bypass. The classification

https://doi.org/10.1017/S0016756822000693

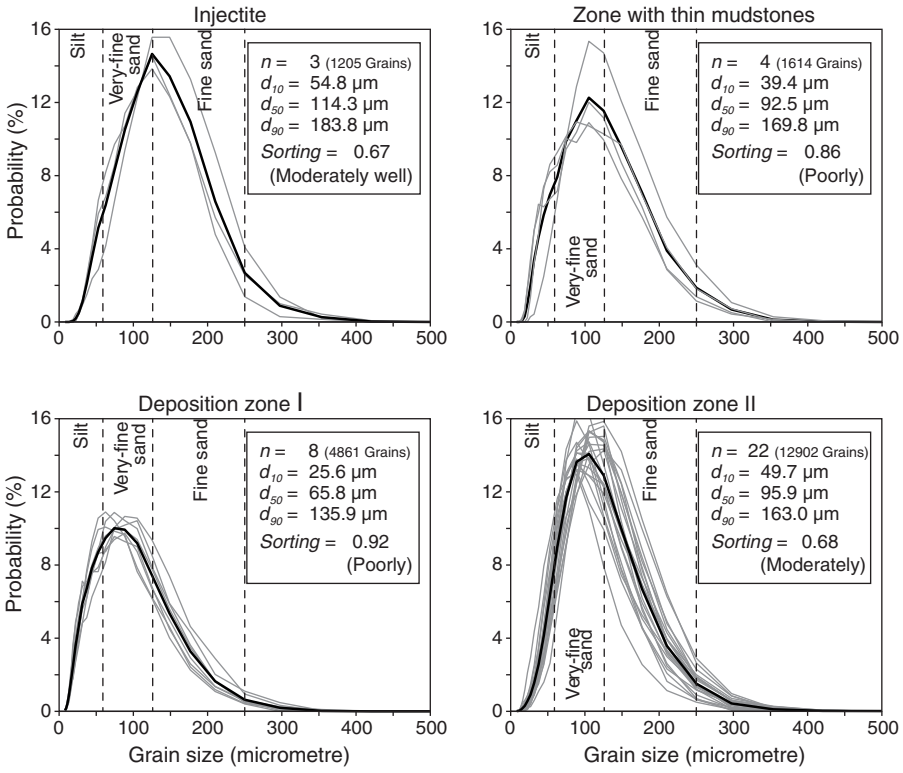

Fig. 11. Grain-size distributions of the samples obtained by image analysis from thin-sections. Sample locations are shown in Figure 9a. The grey lines mark the grain-size distribution of individual samples. The black line marks the average grain-size distribution of all individual samples at that location.

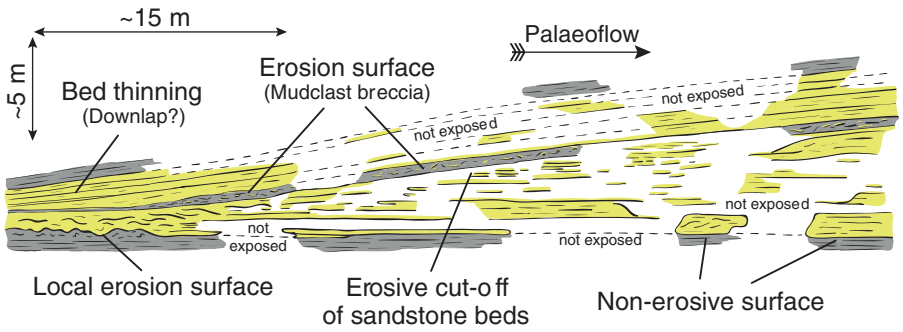

Fig. 12. (Colour online) Sketch of the transition from the bypass zone to the deposition zone (see Fig. 2 for location). The beds in the lower part of Unit E are cut off and draped by a mudclast breccia, which is dipping upstream. Sandstone beds on top of the mudclast breccia are thinning upwards and laterally in the upstream direction.

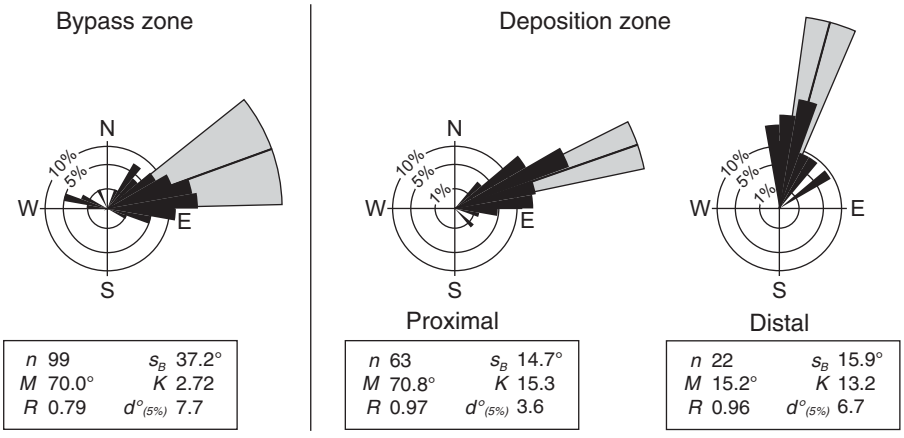

Fig. 13. Equal-area rose diagrams of the palaeoflow measurements in the outcrop complex. Palaeoflow directions in the distal deposition zone deviate from the direction in the proximal deposition zone and in the bypass zone (see Fig. 14 for location). Furthermore, the palaeoflow direction in the bypass zone shows a higher variability than the flows in the lobe. The grey sector describes the mean vector orientation (black line) and length (sector length), and the circular standard deviation (sector width). *M*: mean vector; *R*: Mean vector length; s_B: Circular standard deviation; *K*: Vectorial concentration; *d°*: Confidence interval of the mean vector. Statistics and equal-area rose diagrams were calculated with EZ-ROSE (Baas, 2000).

https://doi.org/10.1017/S0016756822000693

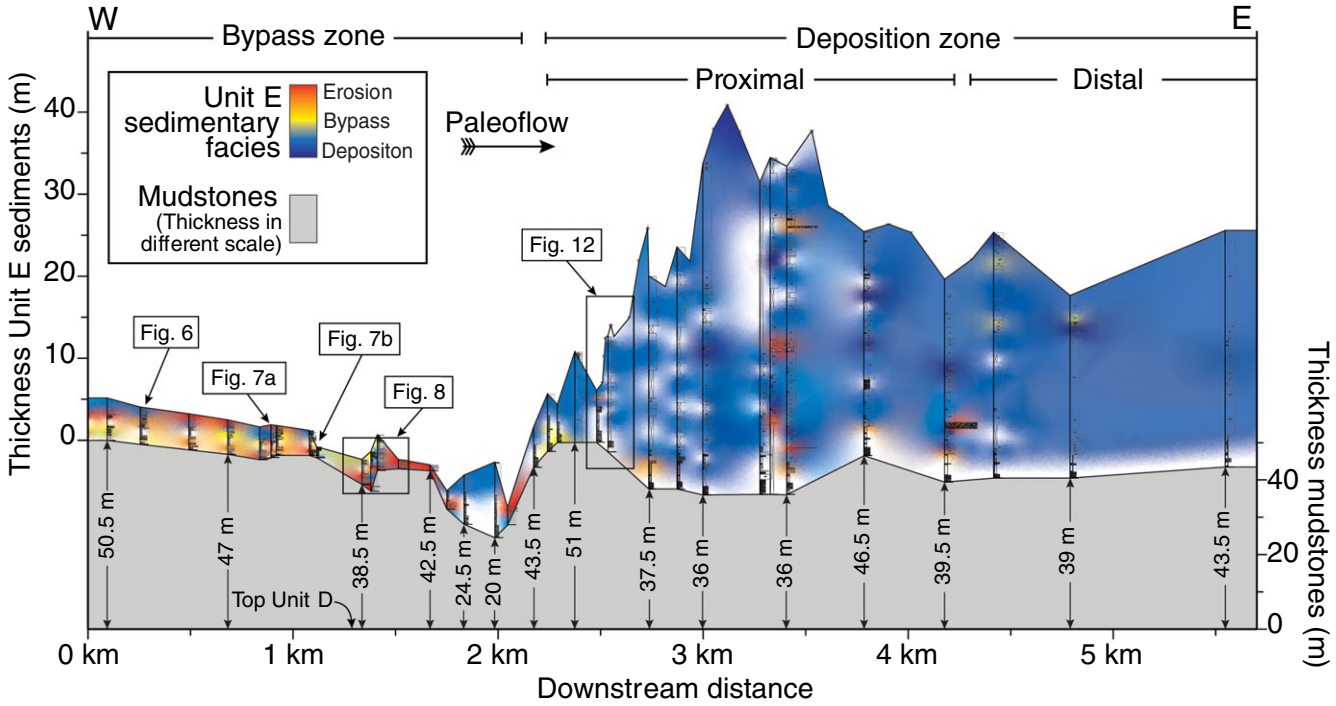

Fig. 14. (Colour online) Correlation panel of Unit E showing the measured sections and the dominant sedimentary facies in the colour scheme of Figure 5. Palaeoflow direction is from left (W) to right (E) and oriented broadly parallel with the alignment of the sections. The bypass zone is characterized by thinner deposits and erosive sedimentary facies. Further downstream the onset of deposition is recorded, reflected by a significant increase of deposit thickness and a deposition zone marked by thicker deposits and sedimentary facies that are indicative of fast deposition.

presented in this paper emphasizes this erosion, bypass and deposition. It can thus be seen as a complementary axis to Mutti's (1992) process perspective on turbidite sandstones.

Lowe (1982) established a more detailed scheme with special reference to high-density turbidity current deposits. The focus of this landmark publication is a careful correlation between depositional processes in high-density turbidity currents and deposit characteristics. Erosion and bypass is present implicitly in this facies scheme due to its focus on deposition. Scour surfaces at the base of beds are unspecified, wavy surfaces overlain directly by gravelly and sandy facies. Eroded mudstone clasts are incorporated in some of the facies. They are primarily included towards the top of idealized event beds, where they give reason to infer cohesive flow processes (Lowe, 1982). This is a contrast to the scheme presented here, in which mudclasts are commonly preserved in close association to scour surfaces (Figs 4h, 7, 8). The association of mudclast horizons with scouring was also observed in active seafloor systems (Carvajal *et al.* 2017; Maier *et al.* 2020; Fildani *et al.* 2021). This contrast to the scheme of Lowe (1982) could indicate that the latter scheme is tailored to positions down-dip of the CLTZ, further away from erosion loci, presumably scaling with the size of the CLTZ.

A striking aspect of this comparison is that previous publications associate erosion and bypass with coarse-grained deposits, commonly with pebbles and cobbles, and almost without exception containing coarse-grained sand – granules (F2–7 of Mutti; S1 of Lowe). This correlation can be correct, and is based in the intuitive reasoning that stronger flows have both the competence to transport larger sediment particles and the capacity to erode more sediment. Our study, however, was performed in the Permian Fort Brown Formation of the Karoo Basin. Even the sandy turbidites here seldom contain grains as coarse as coarse sand (Figs 9b, 11). Yet, the process-based facies scheme demonstrates ample evidence for highly dynamic and erosive behaviour despite this lack of coarse-grained source material. This insight highlights that grain-size and process dynamics cannot always be correlated one-to-one. Systems in which supply of coarse material is limited can still experience strong flows with erosive ability.

In summary, the classification scheme presented here is complementary to previous schemes and seafloor observations. It generally expands the range of features that can be interpreted as indicators of erosion and bypass, where previous schemes emphasize deposition. This makes the scheme especially useful as an additional tool to characterize deposits in CLTZs and for fine-grained systems, respectively.

5.b. Interpretation of the sedimentary structures and architectures

5.b.1. Thinning of the mudstone package underneath Unit E: a mega-scour?

The decrease in thickness of the mudstone package separating Unit E from Unit D defined by using GPS data and satellite images suggests that this zone reflects a local depression in the palaeo-bathymetry (Figs 8a, 9a). A decrease in thickness of the mudstone package between Units D and E was also recognized in a previous study by Brooks *et al.* (2018*a*). However, in contrast to the findings of the present study, Brooks *et al.* (2018*a*) describe an abrupt, rather than a gradual, thinning of the mudstone package. In addition, they also describe a fanning pattern of beds within the mudstones with a thickness increase toward the W (see fig. 11 in Brooks *et al.* 2018*a*). Based on those observations, Brooks *et al.* (2018*a*) interpreted the thickness of the mudstones to reflect a depression in the palaeo-bathymetry caused by a listric syn-sedimentary

https://doi.org/10.1017/S0016756822000693

normal fault that ends in a zone of detachment between Units D and E. Indeed, seafloor data from the Navy Fan suggest that scouring can be controlled by activity and location of faults (Carvajal *et al.* 2017).

An alternative interpretation is suggested here, which interprets the local depression in the palaeo-bathymetry as a mega-scour. The dimensions of this scour with a length of ~500 m and an incision depth of ~25 m are similar to those of scours observed in CLTZs on the modern ocean floor, and in some cases are related to fault activity (Normark *et al.* 1979, 2009; Kenyon & Millington, 1995; Migeon *et al.* 2001; Wynn *et al.* 2002; Macdonald *et al.* 2011; Carvajal *et al.* 2017; Maier *et al.* 2020). The asymmetric shape of the infill of the scour, as well as the location within the bypass zone are further aspects that are consistent with a scour interpretation. Scours of similar size and shape have been observed adjacent to the channel thalweg in seafloor datasets (Carvajal *et al.* 2017; Maier *et al.* 2020; Fildani *et al.* 2021). In contrast, scours within the channel thalweg of modern systems tend to be significantly larger in the order of 1–2 km (Carvajal *et al.* 2017; Heijnen *et al.* 2020; Maier *et al.* 2020; Fildani *et al.* 2021). After their formation such scours can remain unfilled ('open') for over 0.2 Ma without capturing significant amounts of sediment (Macdonald *et al.* 2011). Common sedimentary facies associated with large scours are fine-grained, thin-bedded and structured sediments with several internal erosive horizons draping a major erosion surface (Macdonald *et al.* 2011; Hofstra *et al.* 2015; Stevenson *et al.* 2015). We were not able to identify a distinct erosion surface underneath, or erosive horizons within the thin bedded fine-grained sandstones at the base of the scour. However, the type and structure of the scour infill are similar to the structures observed in push cores taken from scour surfaces in the Navy Fan (Carvajal *et al.* 2017). In addition, highly erosive flows might have emplaced the injectites upstream of the scour showing the coarsest grain-size distribution of all sampling locations (Figs 9b, 11). Nevertheless, the deposits at the base of the scour seem to represent sediments that were captured within the scour during the period it was kept open and underfilled.

On top of the thin-bedded fine-grained sandstones lies a 3.5 m thick structureless and poorly sorted sandstone. These sediments are interpreted as the deposits from turbidity currents that were collapsing upon flowing into the scour depression, resulting in the poor grain-size sorting of the deposited sand (Fig. 11).

After the shutdown of the sediment supply and the end of deposition of Unit E the scour still represented a depression on the ocean floor and was draped and filled with hemipelagic mud and silt-sized deposits from small turbidity currents.

5.b.2. Incision in the bypass zone

The ~20 m long, ~2 m deep incision in the bypass zone is interpreted as a scour (Fig. 6). This interpretation is based on the shape of the incision, the association with the sedimentary facies and structures, and the grain-size distribution of the collected samples. Based on these data, different phases of the development and evolution of the scour have been reconstructed (Fig. 15).

Phases 1 and 2: The scour was cut into the underlying mudstone by a highly erosive turbidity current, where a local defect in the ocean floor might have facilitated the formation of the scour at this particular location (see 'defect model' in Allen, 1971). This local defect could have looked like the locally eroded and ripped seafloor as observed in other locations in the bypass zone (Fig. 7a, b). The turbidity current that was incising the scour probably also emplaced the two injectites underneath and downstream of the scour (*sensu* Eggenhuisen *et al.* 2011) as suggested by their similar

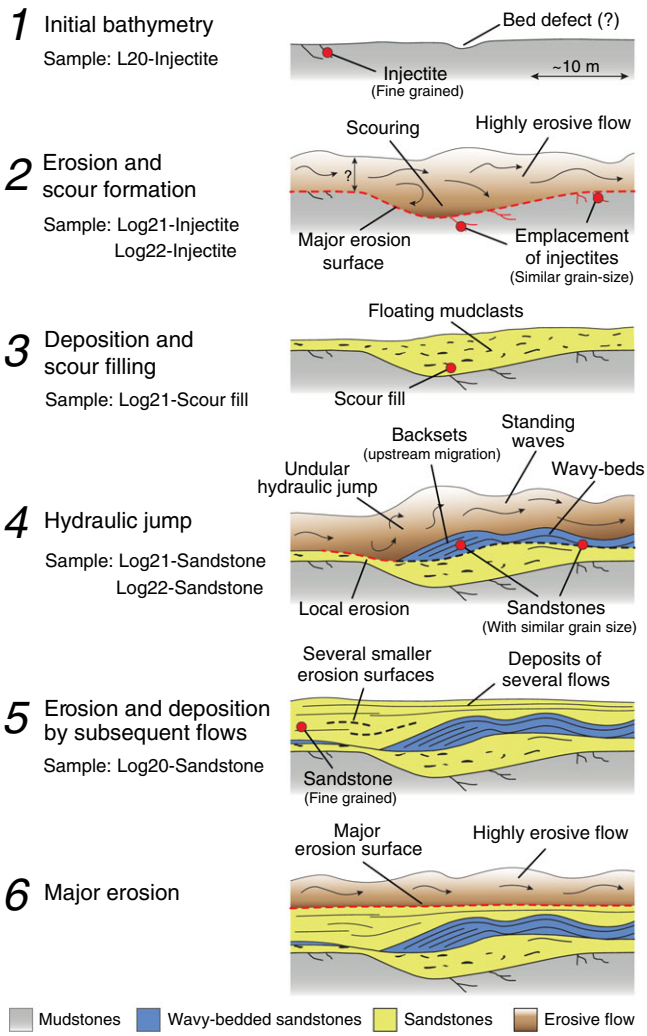

Fig. 15. (Colour online) Phases of the development and evolution of the incision in the bypass zone shown in Figure 8.

grain-size distribution (Fig. 8). The injectite farther upstream of the scour shows a finer grain-size distribution and is therefore probably related to a previous turbidity current (Fig. 15).

Phase 3: After its incision, the scour was filled with sand and mudclasts. It is not clear whether the infill of the scour is related to the same turbidity current event that incised the scour. However, the finer grain-size distribution of the sandstone within the scour compared to that of the injectites underneath suggests that the scour was filled by one or multiple subsequent flows (Figs 8, 15).

Phase 4: The next phase was characterized by the deposition of the backsets and the wavy beds further downstream (Fig. 15). Backsets are typical for bedforms resulting from an upstream-migrating hydraulic jump (e.g. Macdonald *et al.* 2009; Cartigny *et al.* 2014; Vellinga *et al.* 2018). The wavy beds immediately downstream of the backsets are interpreted to have been deposited by standing waves that typically form downstream of undular hydraulic jumps (e.g. Lennon & Hill, 2006; Cartigny *et al.* 2014; Slootman *et al.* 2016, 2018). Grain-size samples from the backsets and the wavy beds show a similar grain-size distribution, supporting the (cor)relation of these two. Experiments demonstrate the formation of hydraulic jumps in scenarios where deposits formed a slope with an adverse gradient (Pohl *et al.* 2020*a*). It is likely that

https://doi.org/10.1017/S0016756822000693

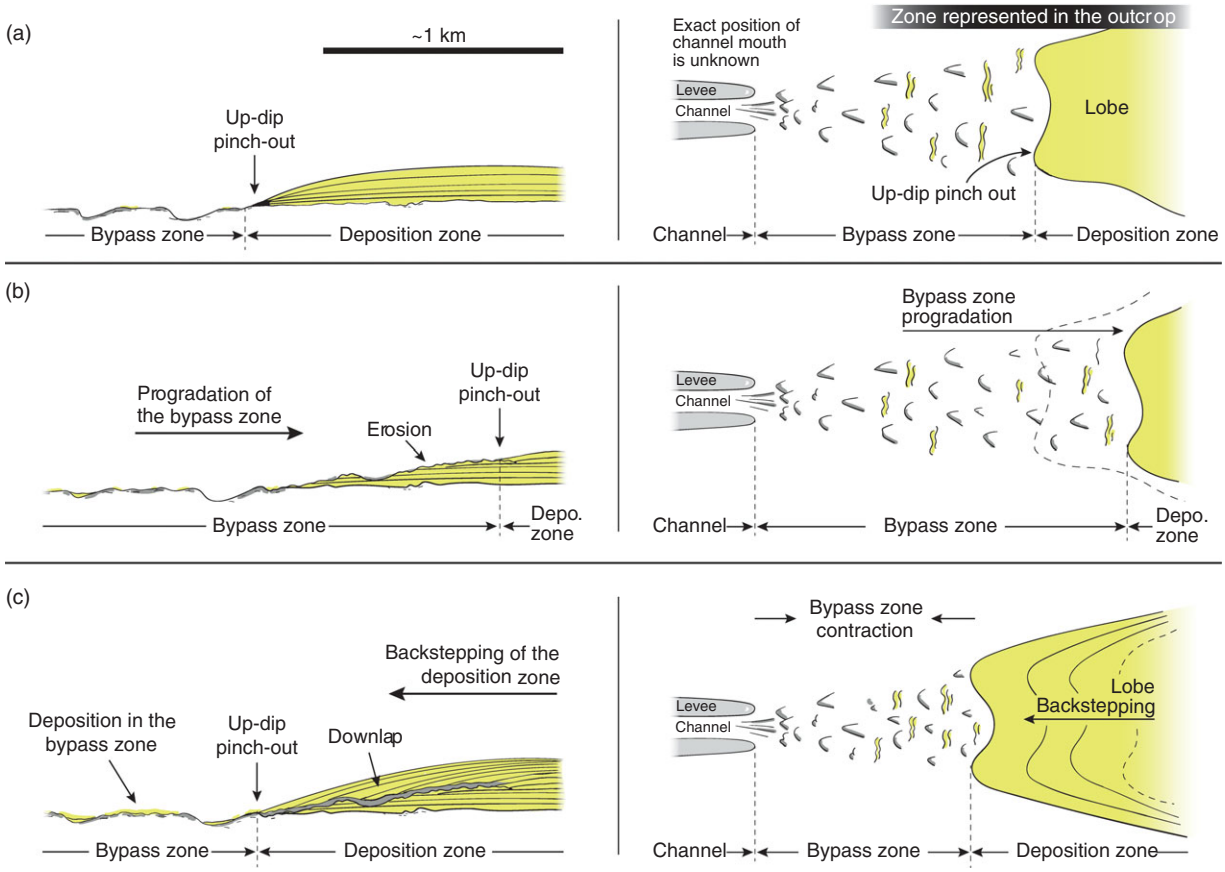

Fig. 16. (Colour online) Reconstruction of the progradation and backstepping of the bypass zone. (a) During the first phase, the bypass zone marked by erosion is followed down-dip by the depositional zone. In the depositional zone the contact of the sandstones to the underlying mudstones is mainly depositional with only local erosion. (b) The second phase, where establishment of the systems resulted in a propagation of the bypass zone across the depositional zone. (c) In the third phase a decrease of the system's activity resulted in the backstepping of the deposits and a contraction of the bypass zone.

the hydraulic jump in this fourth phase of the scour evolution was triggered by deposits downstream of the scour (i.e. a topographic rampart) forming a slope with an adverse gradient.

Phases 5 and 6: The fifth phase is characterized by erosion and deposition due to several subsequent flows (Fig. 15). The bathymetry that was formed by the previous phases was draped and filled by several sandstone beds showing multiple small erosion surfaces, suggesting that this phase was dominated by depositional and less erosive flows (Fig. 8). The following, sixth phase is characterized by a major erosion surface that can be traced over the entire length/width of the outcrop (Fig. 8). This erosion surface was formed by a highly erosive turbidity current, probably similar to the flow that was incising the scour in the second phase. The erosive horizon is covered by a thin sandstone bed covered by mudstones indicating low-energy sedimentation and a decrease in sediment supply.

5.b.3. Transition from the bypass to the deposition zone

The architecture of the bedding exactly at the transition between the bypass and the deposition zone reveals three phases of sedimentation and erosion. In the first phase, sediment was deposited as tabular and mainly structureless sandstones. At this location, the character of the contact of the deposits of this phase with the underlying mudstones is mainly depositional with only local erosion, suggesting low- to non-erosive turbidity currents (Figs 12, 16a). The second phase describes the progradation of the bypass zone across the deposition zone (Fig. 16b). The deposits of the first phase were partly eroded by subsequent flows, resulting in an upstream-dipping major erosive surface and a cut-off of the underlying sandstone beds (Fig. 12). The amount of sediment, and the thickness of the stratigraphy which was eroded during the second phase, is unknown. The erosive surface was draped with an up to 0.5 m thick mudclast breccia, which is interpreted to represent the end of the second erosive phase (Fig. 12). In the third phase the mudclast breccia was draped with sandstone beds with an upwards-thinning pattern, suggesting a decrease in system activity and sediment supply or a lateral shift of the system (Fig. 16c). In addition, the sandstone beds show upstream thinning, and a backstepping of the deposition zone. At the end of the third phase, sediment supply was shut off, resulting in deposition of hemipelagic mud.

5.c. Palaeoflow distribution

In the bypass zone and the proximal deposition zone, the main palaeoflow direction is toward the ENE (~70°), suggesting the connection of these two zones. (Fig. 13). The variability in palaeoflow direction between these two zones is different. The higher variability in the bypass zone ($s_B = 37.2°$; Fig. 13) could be explained by bathymetric irregularities of the seabed such as scours or focal points of deposition. These irregularities steer the gravity-driven turbidity currents toward depressions in the ocean floor, resulting in local changes in flow direction over short distances (e.g. Eggenhuisen *et al.* 2010). The presence of these irregularities in the bathymetry is supported by our field observations of substantial seabed erosion and scouring in the bypass zone (e.g. Figs 6, 7,

https://doi.org/10.1017/S0016756822000693

8). In contrast, the lower variability in palaeoflow direction in the deposition zone ($s_B = 14.7°$; Fig. 13) suggests less local topographic steering and a less irregular seabed. This is supported by the predominantly flat tops of the sandstone beds that were deposited in the deposition zone, implying a flat and uniform ocean floor rather than irregularities. The increased variability in palaeoflow direction may represent an additional criterion to identify zones of bypass and erosion in sparse datasets. However, for this assessment a significant number of reliable palaeoflow indicators would be required. Palaeoflow indicators used for this study are grooves and flutes, which are commonly associated with fast and stronger flows that are capable of leaving marks in the seabed (Peakall *et al.* 2020). Depositional flows might not leave such palaeoflow indicators, especially flutes (Peakall *et al.* 2020). Thus, our palaeoflow results would only capture the direction of the fast and strong flows in the depositional zone. Predominantly depositional or even collapsing flows might have a higher variability in palaeoflow direction, but that would not be documented in flute and groove marks. The measured palaeoflow indicators were commonly found at the base of sandstone beds that were decimetres thick, and displayed facies characteristic for the depositional zone (Fig. 4c). This indicates that at least the flutes and grooves were representative of part of the depositional flows in this zone.

Palaeoflow measurements show a change in the mean direction from ENE in the bypass zone and the proximal deposition zone to NNE in the distal deposition zone (Fig. 13). We suggest two different explanations for the change in mean flow direction. First, the change could have been caused by topographic steering of the turbidity currents. In this scenario a bathymetric high formed by sediment accumulations deposited by former turbidity currents forced a change in mean flow direction. Such variability in palaeoflow direction is also commonly observed in high-resolution modern seafloor data (Carvajal *et al.* 2017; Maier *et al.* 2020). Second, the turbidity currents flowing out into the depositional zone might be more readily diverted by oceanographic effects such as contour currents or geostrophic flow that were flowing along slope to the NW. This effect has recently been brought to attention in literature on other datasets (Fuhrmann *et al.* 2020; Miramontes *et al.* 2020). While there is no documentation yet of deposits that would suggest the existence of geostrophic flows or contour current activity in the Permian Karoo Basin, this interpretation would be consistent with the position on the western margin of a large marine body of water at a palaeolatitude of 60° on the Southern Hemisphere in the Permian (Van Hinsbergen *et al.* 2015).

6. Conclusions

This study provides documentation of detailed sedimentary characteristics that indicate zones dominated by sediment bypass and erosion applicable for identifying CLTZs in other datasets, such as outcrops with limited palaeogeographical context and sediment cores obtained from subsurface systems, and to make predictions away from points of control in sparse datasets.

A process-based facies classification scheme was developed allowing us to distinguish zones of bypass from zones of deposition by sedimentary facies on a bed scale rather than from the overall thickens of the deposits. In the bypass zone, sediment facies were dominated by erosion but show a complex alternation with depositional structures. Common erosive facies were mudclast breccias, injectites, and amalgamated beds with mudclast. Typical depositional facies were rippled and laminated beds, structureless sandstones and convoluted beds. In contrast to the bypass zone, the depositional zone was dominated by depositional facies, and erosive facies could only be recognized occasionally. The spatial distribution and frequency of process-based sedimentary facies can provide a criterion to identify zones of erosion and deposition in other datasets.

Metre-scale structures in the bypass zone indicate highly erosive turbidity currents resulting in ocean-floor erosion and scour formation. In the specific outcrop, GPS data and field relations suggest the presence of a ~500 m long scour. Such scours are difficult to identify in outcrop but represent common features in CLTZs identified in seafloor bathymetry. This study provides an example how a ~500 m long scour could be identified based on field relations and sedimentary facies.

In addition to facies associations and large-scale structures, zones of bypass could also be identified based on variation in the local palaeoflow direction. In the bypass zone the variation in palaeoflow direction was higher than in the depositional zone. This increased variability may be attributed to topographic steering of the turbidity currents due to irregularities on the seabed such as scours or focal points of deposition. However, variations of the palaeoflow distribution could only serve as a potential criterion to identify zones of bypass if a significant number of reliable palaeoflow measurements is available.

The here presented process-based documentation of CLTZ features can help to identify areas dominated by bypass or erosion in sparse datasets with limited palaeogeographic context encountered elsewhere.

Supplementary material. To view supplementary material for this article, please visit https://doi.org/10.1017/S0016756822000693

Acknowledgements. This contribution is part of EuroSEDS (Eurotank Studies of Experimental Deepwater Sedimentology), supported by the NWO (Netherlands Organization for Scientific Research) (grant no. NWO 864.13.006), ExxonMobil, Shell and Equinor. We thank the local farmers of the Laingsburg region for permission to undertake field studies on their land, especially Henk Steyn. Katherine Maier, Cristian Carvajal, Andrea Fildani and Editor Peter Clift provided detailed and constructive reviews that helped us to improve our paper.

Conflict of interest. None.

References

Allen JRL (1970) A quantitative model of climbing ripples and their cross-laminated deposits. *Sedimentology* **14**, 5–26.

Allen JRL (1971) Transverse erosional marks of mud and rock: their physical basis and geological significance. *Sedimentary Geology* **5**, 167–385.

Allen JRL (1972) Intensity of deposition from avalanches and the loose packing of avalanche deposits. *Sedimentology* **18**, 105–11.

Allen JRL (1973) A classification of climbing-ripple cross-lamination. *Journal of the Geological Society* **129**, 537–41.

Altinakar MS, Graf WH and Hopfinger EJ (1996) Flow structure in turbidity currents. *Journal of Hydraulic Research* **34**, 713–18.

Amy LA (2019) A review of producing fields inferred to have upslope stratigraphically trapped turbidite reservoirs: trapping styles (pure and combined), pinchout formation and depositional setting. *AAPG Bulletin* **103**, 2861–89.

Anderton R (1985) Clastic facies models and facies analysis. In *Sedimentology: Recent Developments and Applied Aspects* (eds. PJ Brenchley and BPJ Williams), pp. 31–47. Blackwell Publishing Ltd.

Baas JH (1994) A flume study on the development and equilibrium morphology of current ripples in very fine sand. *Sedimentology* **41**, 185–209.

Baas JH (2000) EZ-ROSE: a computer program for equal-area circular histograms and statistical analysis of two-dimensional vectorial data. *Computers and Geosciences* **26**, 153–66.

Boggs SJ (2009) Petrology of sedimentary rocks. In *Petrology of Sedimentary Rocks* (ed SJ Boggs), pp. 21–49. Cambridge: Cambridge University Press.

Bouma AH (1962) *Sedimentology of Some Flysch Deposits; A Graphic Approach to Facies Interpretation*. Amsterdam: Elsevier,, 168 pp.

Breien H, De Blasio FV, Elverhoi A, Nystuen JP and Harbitz CB (2010) Transport mechanisms of sand in deep-marine environments: —insights based on laboratory experiments. *Journal of Sedimentary Research* **80**, 975–90.

Brooks HL, Hodgson DM, Brunt RL, Peakall J, Hofstra M and Flint SS (2018a) Deep-water channel-lobe transition zone dynamics: processes and depositional architecture, an example from the Karoo Basin, South Africa. *GSA Bulletin* **130**, 1723–46.

Brooks HL, Hodgson DM, Brunt RL, Peakall J, Poyatos-Moré M and Flint SS (2018b) Disconnected submarine lobes as a record of stepped slope evolution over multiple sea-level cycles. *Geosphere* **14**, 1753–79.

Butler RWH and McCaffrey WD (2010) Structural evolution and sediment entrainment in mass-transport complexes: outcrop studies from Italy. *Journal of the Geological Society* **167**, 617–31.

Cartigny MJB, Ventra D, Postma G and van Den Berg JH (2014) Morphodynamics and sedimentary structures of bedforms under supercritical-flow conditions: new insights from flume experiments. *Sedimentology* **61**, 712–48.

Carvajal C, Paull CK, Caress DW, Fildani A, Lundsten E, Anderson K, Maier KL, McGann M, Gwiazda R and Herguera JC (2017) Unraveling the channel-lobe transition zone with high-resolution AUV bathymetry: Navy Fan, offshore Baja California, Mexico. *Journal of Sedimentary Research* **87**, 1049–59.

Catuneanu O, Hancox PJ and Rubidge BS (1998) Reciprocal flexural behaviour and contrasting stratigraphies: a new basin development model for the Karoo retroarc foreland system, South Africa. *Basin Research* **10**, 417–39.

Cobain SL, Hodgson DM, Peakall J and Shiers MN (2017) An integrated model of clastic injectites and basin floor lobe complexes: implications for stratigraphic trap plays. *Basin Research* **29**, 816–35.

Cobain SL, Peakall J and Hodgson DM (2015) Indicators of propagation direction and relative depth in clastic injectites: implications for laminar versus turbulent flow processes. *Bulletin of the Geological Society of America* **127**, 1816–30.

Collinson J, Mountney NP and Thompson D (2006) *Sedimentary Structures*, 3rd edn. Edinburgh: Dunedin Academic Press, 304 pp.

Di Celma CN, Brunt RL, Hodgson DM, Flint SS and Kavanagh JP (2011) Spatial and temporal evolution of a Permian submarine slope channel-Levee system, Karoo Basin, South Africa. *Journal of Sedimentary Research* **81**, 579–99.

Earle S (2019) *Physical Geology*, 2nd edn. Victoria, BC: BCcampus, 827 pp.

Eggenhuisen JT, McCaffrey WD, Haughton PDW and Butler RWH (2010) Small-scale spatial variability in turbidity-current flow controlled by roughness resulting from substrate erosion: field evidence for a feedback mechanism. *Journal of Sedimentary Research* **80**, 129–36.

Eggenhuisen JT, McCaffrey WD, Haughton PDW and Butler RWH (2011) Shallow erosion beneath turbidity currents and its impact on the architectural development of turbidite sheet systems. *Sedimentology* **58**, 936–59.

Figueiredo JJP, Hodgson DM, Flint SS and Kavanagh JP (2010) Depositional environments and sequence stratigraphy of an exhumed Permian mudstone-dominated submarine slope succession, Karoo Basin, South Africa. *Journal of Sedimentary Research* **80**, 97–118.

Figueiredo JJP, Hodgson DM, Flint SS and Kavanagh JP (2013) Architecture of a channel complex formed and filled during long-term degradation and entrenchment on the upper submarine slope, Unit F, Fort Brown Fm., SW Karoo Basin, South Africa. *Marine and Petroleum Geology* **41**, 104–16.

Fildani A, Drinkwater NJ, Weislogel A, McHargue T, Hodgson DM and Flint SS (2007) Age controls on the Tanqua and Laingsburg deep-water systems: new insights on the evolution and sedimentary fill of the Karoo Basin, South Africa. *Journal of Sedimentary Research* **77**, 901–8.

Fildani A, Hubbard SM, Covault JA, Maier KL, Romans BW, Traer M and Rowland JC (2013) Erosion at inception of deep-sea channels. *Marine and Petroleum Geology* **41**, 48–61.

Fildani A, Kostic S, Covault JA, Maier KL, Caress DW and Paull CK (2021) Exploring a new breadth of cyclic steps on distal submarine fans. *Sedimentology* **68**, 1378–99.

Flint SS, Hodgson DM, Sprague AR, Brunt RL, Van der Merwe WC, Figueiredo J, Prélat A, Box D, Di Celma C and Kavanagh JP (2011) Depositional architecture and sequence stratigraphy of the Karoo basin floor to shelf edge succession, Laingsburg depocentre, South Africa. *Marine and Petroleum Geology* **28**, 658–74.

Fuhrmann A, Kane IA, Clare MA, Ferguson RA, Schomacker E, Bonamini E and Contreras FA (2020) Hybrid turbidite-drift channel complexes: an integrated multiscale model. *Geology* **48**, 562–8.

Galy V, France-Lanord C, Beyssac O, Faure P, Kudrass H and Palhol F (2007) Efficient organic carbon burial in the Bengal fan sustained by the Himalayan erosional system. *Nature* **450**, 407–10.

Gardner MH, Borer JM, Melick JJ, Mavilla N, Dechesne M and Wagerle RN (2003) Stratigraphic process-response model for submarine channels and related features from studies of Permian Brushy Canyon outcrops, West Texas. *Marine and Petroleum Geology* **20**, 757–87.

Haughton P, Davis C, McCaffrey W and Barker S (2009) Hybrid sediment gravity flow deposits: classification, origin and significance. *Marine and Petroleum Geology* **26**, 1900–18.

Haughton PDW, Barker SP and McCaffrey WD (2003) 'Linked' debrites in sand-rich turbidite systems: origin and significance. *Sedimentology* **50**, 459–82.

Heijnen MS, Clare MA, Cartigny MJB, Talling PJ, Hage S, Lintern DG, Stacey C, Parsons DR, Simmons SM, Chen Y, Sumner EJ, Dix JK and Hughes Clarke JE (2020) Rapidly-migrating and internally-generated knickpoints can control submarine channel evolution. *Nature Communications* **11**, 1–15.

Hessler AM and Fildani A (2019) Deep-sea fans: tapping into Earth's changing landscapes. *Journal of Sedimentary Research* **89**, 1171–9.

Hodgson DM (2009) Distribution and origin of hybrid beds in sand-rich submarine fans of the Tanqua depocentre, Karoo Basin, South Africa. *Marine and Petroleum Geology* **26**, 1940–56.

Hodgson DM, Di Celma CN, Brunt RL and Flint SS (2011) Submarine slope degradation and aggradation and the stratigraphic evolution of channel-levee systems. *Journal of the Geological Society* **168**, 625–8.

Hodgson DM, Kane IA, Flint SS, Brunt RL and Ortiz-Karpf A (2016) Time-transgressive confinement on the slope and the progradation of basin-floor fans: implications for the sequence stratigraphy of deep-water deposits. *Journal of Sedimentary Research* **86**, 73–86.

Hofstra M, Hodgson DM, Peakall J and Flint SS (2015) Giant scour-fills in ancient channel-lobe transition zones: formative processes and depositional architecture. *Sedimentary Geology* **329**, 98–114.

Hubbard SM, Covault JA, Fildani A and Romans BW (2014) Sediment transfer and deposition in slope channels: deciphering the record of enigmatic deep-sea processes from outcrop. *Bulletin of the Geological Society of America* **126**, 857–71.

Hurst A, Cartwright J, Huuse M, Jonk R, Schwab A, Duranti D and Cronin B (2003) Significance of large-scale sand injectites as long-term fluid conduits: evidence from seismic data. *Geofluids* **3**, 263–74.

Ito M, Ishikawa K and Nishida N (2014) Distinctive erosional and depositional structures formed at a canyon mouth: a lower Pleistocene deep-water succession in the Kazusa forearc basin on the Boso Peninsula, Japan. *Sedimentology* **61**, 2042–62.

Jobe ZR, Lowe DR and Morris WR (2012) Climbing-ripple successions in turbidite systems: depositional environments, sedimentation rates and accumulation times. *Sedimentology* **59**, 867–98.

Jobe ZR, Sylvester Z, Howes N, Pirmez C, Parker A, Cantelli A, Smith R, Wolinsky MA, O'Byrne C, Slowey N and Prather B (2017) High-resolution, millennial-scale patterns of bed compensation on a sand-rich intraslope submarine fan, western Niger Delta slope. *Bulletin of the Geological Society of America* **129**, 23–37.

https://doi.org/10.1017/S0016756822000693

Johnson M (1994) Thin-section grain size analysis revised. *Sedimentology* **41**, 985–99.

Johnson MR (1991) Sandstone petrography, provenance and plate tectonic setting in Gondwana context of the southeastern Cape-Karoo Basin. *South African Journal of Geology* **94**, 137–54.

Jones GED, Hodgson DM and Flint SS (2015) Lateral variability in clinoform trajectory, process regime, and sediment dispersal patterns beyond the shelf-edge rollover in exhumed basin margin-scale clinothems. *Basin Research* **27**, 657–80.

Kane IA (2010) Development and flow structures of sand injectites: the Hind Sandstone Member injectite complex, Carboniferous, UK. *Marine and Petroleum Geology* **27**, 1200–15.

Kenyon NH and Millington J (1995) Contrasting deep-sea depositional systems in the Bering Sea. In *Atlas of Deep Water Environments* (eds KT Pickering, RN Hiscott, NH Kenyon, F Ricci Lucchi and RDA Smith), pp. 196–202. Dordrecht: Springer Netherlands.

Kneller B (1995) Beyond the turbidite paradigm: physical models for deposition of turbidites and their implications for reservoir prediction. In *Characterization of Deep Marine Clastic Systems* (ed. AJ Hartley), pp. 31–49. *Geological Society of London, Special Publication no. 94* .

Kneller BC and Branney MJ (1995) Sustained high-density turbidity currents and the deposition of thick massive sands. *Sedimentology* **42**, 607–16.

Kuenen PH (1937) Experiments in connection with Daly's hypothesis on the formation of submarine canyons. *Leidsche Geologische Mededeelingen* **7**, 327–51.

Lennon JM and Hill DF (2006) Particle image velocity measurements of undular and hydraulic jumps. *Journal of Hydraulic Engineering* **132**, 1283–94.

Lien T, Midtbø RE and Martinsen OJ (2006) Depositional facies and reservoir quality of deep-marine sandstones in Norwegian Sea. *Norwegian Journal of Geology* **86**, 71–92.

López Gamundí OR and Rossello EA (1998) Basin fill evolution and paleotectonic patterns along the Samfrau geosyncline: the Sauce Grande basin-Ventana foldbelt (Argentina) and Karoo basin-Cape foldbelt (South Africa) revisited. *Geologische Rundschau* **86**, 819–34.

Lowe DR (1982) Sediment gravity flows: II. Ddepositional models with special reference to the deposits of high-density turbidity currents. *SEPM Journal of Sedimentary Research* **52**, 279–97.

Macdonald HA, Wynn RB, Huvenne VAI, Peakall J, Masson DG, Weaver PPE and McPhail SD (2011) New insights into the morphology, fill, and remarkable longevity (>0.2 m.y.) of modern deep-water erosional scours along the northeast Atlantic margin. *Geosphere* **7**, 845–67.

Macdonald RG, Alexander J, Bacon JC and Cooker MJ (2009) Flow patterns, sedimentation and deposit architecture under a hydraulic jump on a non-eroding bed: defining hydraulic-jump unit bars. *Sedimentology* **56**, 1346–67.

Maier KL, Paull CK, Caress DW, Anderson K, Nieminski NM, Lundsten E, Erwin BE, Gwiazda R and Fildani A (2020) Submarine-fan development revealed by integrated high-resolution datasets from La Jolla fan, offshore California, U.S.A. *Journal of Sedimentary Research* **90**, 468–79.

McKay MP, Weislogel AL, Jackson WT, Dean J and Fildani A (2018) Structural and magmatic controls on the turbidites of the Karoo Basin, South Africa. In *Tectonics, Sedimentary Basins, and Provenance: A Celebration of the Career of William R. Dickinson* (eds RV Ingersoll, SA Graham and TF Lawton), pp. 689–706. Boulder, Colorado: Geological Society of America.

Meiburg E and Kneller B (2010) Turbidity currents and their deposits. *Annual Review of Fluid Mechanics* **42**, 135–56.

Migeon S, Savoye B, Zanella E, Mulder T, Faugères JC and Weber O (2001) Detailed seismic-reflection and sedimentary study of turbidite sediment waves on the Var sedimentary ridge (SE France): significance for sediment transport and deposition and for the mechanisms of sediment-wave construction. *Marine and Petroleum Geology* **18**, 179–208.

Miramontes E, Eggenhuisen JT, Silva Jacinto R, Poneti G, Pohl F, Normandeau A, Campbell DC and Hernández-molina FJ (2020) Channel-Levee evolution in combined contour current–turbidity current flows from flume-tank experiments. *Geology* **48**, 1–5.

Mulder T and Alexander J (2001) The physical character of subaqueous sedimentary density flow and their deposits. *Sedimentology* **48**, 269–99.

Mutti E (1992) *Turbidite Sandstones*: Parma: Agip, Istituto di geologia, Università di Parma, 275 pp.

Mutti E, Bernoulli D, Lucchi FR and Tinterri R (2009) Turbidites and turbidity currents from alpine 'flysch' to the exploration of continental margins. *Sedimentology* **56**, 267–318.

Mutti E and Normark WR (1987) Comparing examples of modern and ancient turbidite systems: problems and concepts. In *Marine Clastic Sedimentology* (eds JK Leggett and GG Zuffa), pp. 1–38. Dordrecht: Springer.

Mutti E, Tinterri R, Remacha E, Mavilla N, Angella S and Fava L (1999) *An Introduction to the Analysis of Ancient Turbidite Basins from an Outcrop Perspective*. AAPG Continuing Education Course Note Series 39. Tulsa, Oklahoma: American Association of Petroleum Geologists, 61pp.

Navarro L and Arnott RW (Bill) C (2020) Stratigraphic record in the transition from basin floor to continental slope sedimentation in the ancient passive-margin Windermere turbidite system. *Sedimentology* 67. doi: 10.1111/sed.12676.

Nemec W (1988) The shape of the rose. *Sedimentary Geology* **59**, 149–52.

Normark WR (1970) Growth patterns of deep-sea fans. *AAPG Bulletin* **54**, 2170–95.

Normark WR, Paull CK, Caress DW, Ussler W and Sliter R (2009) Fine-scale relief related to Late Holocene channel shifting within the floor of the upper Redondo Fan, offshore Southern California. *Sedimentology* **56**, 1690–704.

Normark WR, Piper DJW and Hess GR (1979) Distributary channels, sand lobes, and mesotopography of Navy Submarine Fan, California Borderland, with applications to ancient fan sediments. *Sedimentology* **26**, 749–74.

Ogata K, Mutti E, Pini GA and Tinterri R (2012) Mass transport-related stratal disruption within sedimentary mélanges: examples from the northern Apennines (Italy) and south-central Pyrenees (Spain). *Tectonophysics* **568–569**, 185–99.

Ogata K, Pogačnik Ž, Pini GA, Tunis G, Festa A, Camerlenghi A and Rebesco M (2014) The carbonate mass transport deposits of the Paleogene Friuli Basin (Italy/Slovenia): internal anatomy and inferred genetic processes. *Marine Geology* **356**, 88–110.

Palanques A, Kenyon NH, Alonso B and Limonov A (1996) Erosional and depositional patterns in the Valencia Channel mouth: an example of a modern channel-lobe transition zone. *Marine Geophysical Researches* **18**, 104–18.

Parize O and Fries G (2003) The Vocontian clastic dykes and sills: a geometric model. In *Subsurface Sediment Mobilization* (eds P van Rensbergen, RR Hillis, AJ Maltmah and CK Morley), pp. 51–72. *Geological Society of London, Special Publication* no. 216.

Peakall J, Best J, Baas JH, Hodgson DM, Clare MA, Talling PJ, Dorrell RM and Lee DR (2020) An integrated process-based model of flutes and tool marks in deep-water environments: implications for palaeohydraulics, the Bouma sequence and hybrid event beds. *Sedimentology* **67**, 1601–66.

Pemberton EAL, Hubbard SM, Fildani A, Romans B and Stright L (2016) The stratigraphic expression of decreasing confinement along a deep-water sediment routing system: outcrop example from southern Chile. *Geosphere* **12**, 114–34.

Pickering K, Watson M, Stow D and Hiscott R (1986) Deep-water facies, processes and models: a review and classification scheme for modern and ancient sediments. *Earth-Science Reviews* **23**, 75–174.

Pohl F, Eggenhuisen JT, Cartigny MJB, Tilston MC, de Leeuw J and Hermidas N (2020a) The influence of a slope break on turbidite deposits: an experimental investigation. *Marine Geology* **424**, 106160.

Pohl F, Eggenhuisen JT, Kane IA and Clare MA (2020b) Transport and burial of microplastics in deep-marine sediments by turbidity currents. *Environmental Science & Technology* **54**, 4180–9.

Pohl F, Eggenhuisen JT, Tilston M and Cartigny MJB (2019) New flow relaxation mechanism explains scour fields at the end of submarine channels. *Nature Communications* **10**, 4425.

Poyatos-Moré M, Jones GD, Brunt RL, Hodgson DM, Wild RJ and Flint SS (2016) Mud-dominated basin-margin progradation: processes and implications. *Journal of Sedimentary Research* **86**, 863–78.

Prather BE, Booth JR, Steffens GS and Craig PA (1998) Succession of seismic facies of intraslope basins, deep-water Gulf of Mexico 1. *AAPG Bulletin* **82**, 701–28.

Prather BE, O'Byrne C, Pirmez C and Sylvester Z (2017) Sediment partitioning, continental slopes and base-of-slope systems. *Basin Research* **29**, 394–416.

Prather BE, Pirmez C, Sylvester Z and Prather DS (2012) Stratigraphic response to evolving geomorphology in a submarine apron perched on the upper Niger Delta slope. In *Application of the Principles of Seismic Geomorphology to Continental-Slope and Base-of-Slope Systems: Case Studies from Seafloor and Near-Seafloor Analogues* (eds BE Prather, ME Deptuck, D Mohrig, B van Hoorn and RB Wynn), pp. 145–61., SEPM (Society for Sedimentary Geology), Special Publication 99.

Prélat A, Hodgson DM and Flint SS (2009) Evolution, architecture and hierarchy of distributary deep-water deposits: a high-resolution outcrop investigation from the Permian Karoo Basin, South Africa. *Sedimentology* **56**, 2132–54.

Reading HG (1996) *Sedimentary Environments: Processes, Facies and Stratigraphy*. Chichester: John Wiley & Sons., 704 pp.

Reineck H-E and Singh IB (1980) *Depositional Sedimentary Environment*, 2nd edn. Berlin: Springer, 551 pp.

Scott ED, Bouma AH and Wickens HDEV (2000) Influence of tectonics on submarine fan deposition, Tanqua and Laingsburg Subbasins, South Africa. In *Fine-Grained Turbidite Systems* (eds AH Bouma and CG Stone), pp. 47–56. Tulsa, Oklahoma: American Association of Petroleum Geologists, Memoir 72 and SEPM, Special Publication 68.

Slootman A, Cartigny MJB, Moscariello A, Chiaradia M and de Boer PL (2016) Quantification of tsunami-induced flows on a Mediterranean carbonate ramp reveals catastrophic evolution. *Earth and Planetary Science Letters* **444**, 192–204.

Slootman A, Simpson G, Castelltort S and de Boer PL (2018) Geological record of marine tsunami backwash: the role of the hydraulic jump. *The Depositional Record* **4**, 59–77.

Smith RMH (1990) A review of stratigraphy and sedimentary environments of the Karoo Basin of South Africa. *Journal of African Earth Sciences* **10**, 117–37.

Smith RMH, Eriksson PG and Botha WJ (1993) A review of the stratigraphy and sedimentary environments of the Karoo-aged basins of Southern Africa. *Journal of African Earth Sciences* **16**, 143–69.

Spychala YT, Hodgson DM, Flint SS and Mountney NP (2015) Constraining the sedimentology and stratigraphy of submarine intraslope lobe deposits using exhumed examples from the Karoo Basin, South Africa. *Sedimentary Geology* **322**, 67–81.

Stacey CD, Hill PR, Talling PJ, Enkin RJ, Hughes Clarke J and Lintern DG (2018) How turbidity current frequency and character varies down a fjord-delta system: combining direct monitoring, deposits and seismic data. *Sedimentology* **66**, 1–31.

Stevenson CJ, Jackson CA-L, Hodgson DM, Hubbard SM and Eggenhuisen JT (2015) Deep-water sediment bypass. *Journal of Sedimentary Research* **85**, 1058–81.

Talling PJ, Allin J, Armitage DA, Arnott RWC, Cartigny MJB, Clare MA, Felletti F, Covault JA, Girardclos S, Hansen E, Hill PR, Hiscott RN, Hogg AJ, Hughes Clarke J, Jobe ZR, Malgesini G and Mozzato A (2015) Key future directions for research on turbidity currents and their deposits. *Journal of Sedimentary Research* **85**, 153–69.

Talling PJ, Amy LA, Wynn RB, Peakall J and Robinson M (2004) Beds comprising debrite sandwiched within co-genetic turbidite: origin and widespread occurrence in distal depositional environments. *Sedimentology* **51**, 163–94.

Talling PJ, Masson DG, Sumner EJ and Malgesini G (2012) Subaqueous sediment density flows: depositional processes and deposit types. *Sedimentology* **59**, 1937–2003.

Tankard A, Welsink H, Aukes P, Newton R and Stettler E (2009) Tectonic evolution of the Cape and Karoo basins of South Africa. *Marine and Petroleum Geology* **26**, 1379–412.

van der Merwe WC, Flint SS and Hodgson DM (2010) Sequence stratigraphy of an argillaceous, deepwater basin-plain succession: Vischkuil Formation (Permian), Karoo Basin, South Africa. *Marine and Petroleum Geology* **27**, 321–33.

van der Merwe WC, Hodgson DM, Brunt RL and Flint SS (2014) Depositional architecture of sand-attached and sand-detached channel-lobe transition zones on an exhumed stepped slope mapped over a 2500 km^{2}area. *Geosphere* **10**, 1076–93.

van der Merwe WC, Hodgson DM and Flint SS (2009) Widespread syn-sedimentary deformation on a muddy deep-water basin-floor: the Vischkuil formation (Permian), Karoo Basin, South Africa. *Basin Research* **21**, 389–406.

van der Merwe WC, Hodgson DM and Flint SS (2011) Origin and terminal architecture of a submarine slide: a case study from the Permian Vischkuil Formation, Karoo Basin, South Africa. *Sedimentology* **58**, 2012–38.

Van Hinsbergen DJJ, De Groot LV, Van Schaik SJ, Spakman W, Bijl PK, Sluijs A, Langereis CG and Brinkhuis H (2015) A paleolatitude calculator for paleoclimate studies. *PLOS ONE* **10**, 1–21.

Vellinga AJ, Cartigny MJB, Eggenhuisen JT and Hansen EWM (2018) Morphodynamics and depositional signature of low-aggradation cyclic steps: new insights from a depth-resolved numerical model. *Sedimentology* **65**, 540–60.

Visser JNJ (1997) Deglaciation sequences in the Permo-Carboniferous Karoo and Kalahari basins of southern Africa: a tool in the analysis of cyclic glaciomarine basin fills. *Sedimentology* **44**, 507–21.

Visser JNJ and Loock C (1978) Water depth in the main Karoo Basin, South Africa, during Ecca (Permian) sedimentation. *South African Journal of Geology* **81**, 185–91.

Visser JNJ and Praekelt HE (1996) Subduction, mega-shear systems and Late Palaeozoic basin development in the African segment of Gondwana. *Geologische Rundschau* **85**, 632–46.

Wynn RB, Kenyon NH, Masson DG, Stow DAV and Weaver PPE (2002) Characterization and recognition of deep-water channel-lobe transition zones. *AAPG Bulletin* **86**, 1441–62.

https://doi.org/10.1017/S0016756822000693